Article

Trait-based sensitivity of large mammals to a catastrophic tropical cyclone

Check for updates

Reena H. Walker[1,12], Matthew C. Hutchinson[2,3], Justine A. Becker[2,4], Joshua H. Daskin[5,6], Kaitlyn M. Gaynor[7], Meredith S. Palmer[2], Dominique D. Gonçalves[8,9], Marc E. Stalmans[8], Jason Denlinger[8], Paola Bouley[10,13], Mercia Angela[10], Antonio Paulo[10], Arjun B. Potter[2,14], Nikhail Arumoogum[11], Francesca Parrini[11], Jason P. Marshal[11], Robert M. Pringle[2,15✉] & Ryan A. Long[1,15✉]

Extreme weather events perturb ecosystems and increasingly threaten biodiversity[1]. Ecologists emphasize the need to forecast and mitigate the impacts of these events, which requires knowledge of how risk is distributed among species and environments. However, the scale and unpredictability of extreme events complicate risk assessment[1-4]—especially for large animals (megafauna), which are ecologically important and disproportionately threatened but are wide-ranging and difficult to monitor[5]. Traits such as body size, dispersal ability and habitat affiliation are hypothesized to determine the vulnerability of animals to natural hazards[1,6,7]. Yet it has rarely been possible to test these hypotheses or, more generally, to link the short-term and long-term ecological effects of weather-related disturbance[8,9]. Here we show how large herbivores and carnivores in Mozambique responded to Intense Tropical Cyclone Idai, the deadliest storm on record in Africa, across scales ranging from individual decisions in the hours after landfall to changes in community composition nearly 2 years later. Animals responded behaviourally to rising floodwaters by moving upslope and shifting their diets. Body size and habitat association independently predicted population-level impacts: five of the smallest and most lowland-affiliated herbivore species declined by an average of 28% in the 20 months after landfall, while four of the largest and most upland-affiliated species increased by an average of 26%. We attribute the sensitivity of small-bodied species to their limited mobility and physiological constraints, which restricted their ability to avoid the flood and endure subsequent reductions in the quantity and quality of food. Our results identify general traits that govern animal responses to severe weather, which may help to inform wildlife conservation in a volatile climate.

Extreme climate and weather events—abrupt meteorological phenomena with intensity and/or impact outside normal historical variability—are becoming more frequent and severe[1,10]. Tropical cyclones cause inordinate damage, in large part by triggering catastrophic floods. Although the detection and attribution of storm trends remains challenging, there is growing evidence that the strength and proportion of major tropical cyclones has increased in recent decades, together with extreme rainfall[10-13]. Models predict a high likelihood of further increases in peak cyclone wind speeds, rainfall rates and compound flood risk arising from deluge, storm surge and river flow[10,11]. These factors have prompted urgent calls for research on cyclone ecology to guide forecasts and adaptation plans for biodiversity and ecosystems[1,8,9]. However, the unpredictable nature of severe cyclones makes them difficult to study. Remote sensing and long-term vegetation plots have facilitated assessment of cyclone effects on landscapes[14,15], but there are comparatively few direct studies of animals, most of which involve small-bodied species on oceanic islands[6,7,16-19].

In the 1990s, a series of hurricanes struck small experimental islands in the Bahamas, supplying unusually rich insight into the effects of cyclones on animal communities and showing that species' responses were related to their traits: larger species (lizards) were more resistant to cyclone effects, whereas better dispersers (spiders) recovered

Article

faster[6]. These results hinted at a general trait-based theory of species' robustness—that is, the maintenance (resistance) and recovery (resilience) of normal abundance and behaviour—to climatic catastrophes[7]. Yet the extent to which these principles scale up to large animals in continental systems is unknown.

Unlike comparisons of insular lizards and wind-borne arthropods, body size and dispersal ability are linked in terrestrial mammals[20,21]. As a result, larger species might be both more resistant and more resilient to cyclones. However, alternative possibilities are also plausible. Among large mammalian herbivores and carnivores, most or all species may be sufficiently large and mobile to escape or withstand the acute impacts of extreme weather, and robustness may thus vary little or depend on traits that do not covary with size[22,23]. Over longer timescales, large size might enhance robustness (if lower mass-specific nutritional requirements buffer disruptions of food supply) or reduce it (owing to higher total nutritional requirements and slower reproduction)[24,25]. In light of such uncertainties, recent reviews have stressed the need for process-based understanding of how species' traits regulate responses to cyclones across spatial and temporal scales, and how impacts on populations and communities emerge from processes at lower levels of organization[8,9]. These remain elusive goals; we know of no study that has been able to track the individual-level behavioural mechanisms that underpin community-level responses to cyclones.

Here we investigated how a diverse assemblage of large mammals in Mozambique's Gorongosa National Park responded to Cyclone Idai, one of the most devastating tropical cyclones recorded in the Southern Hemisphere[1,26,27]. The historically abundant megafauna of Gorongosa's mesic savannas (average rainfall, approximately 850 mm yr^{-1}) and productive floodplain grasslands declined by more than 90% during the Mozambican Civil War (1977–1992) but have since recovered considerably[28]. Ongoing long-term research on the movements, distributions, diets and population dynamics of 13 herbivore species—from 17-kg oribi to 4,000-kg elephant—and their predators (lion and African wild dog) provided a unique opportunity to study the impacts of an extreme weather event on a community comprising some of the world's largest terrestrial animals. As in several other African protected areas, large parts of Gorongosa's Rift Valley Basin flood or burn each year[29,30], meaning that resident species have experience with inundation and other disturbances. Using multiple data streams, we compared animal behaviour and performance in the hours, days and months after Cyclone Idai with those observed both immediately before the cyclone and during the corresponding seasonal intervals in normal (non-cyclone) years. We tested two general trait-based hypotheses. First, that species affiliated with wooded, higher-elevation habitats are more robust to cyclones than those affiliated with open, lower-elevation habitat, because the latter is more prone to flooding. Second, that robustness scales positively with body size, because larger mammals have (1) higher mobility and thus can travel farther to escape affected habitats and find food[20,21], and (2) lower mass-specific metabolic rates and thus greater ability to endure the effects of reduced food supply in the months after the storm[25]. Habitat affiliation and body size were uncorrelated ($r = -0.34$, $P = 0.26$; Extended Data Fig. 1), enabling us to evaluate the effects of each trait independently.

Cyclone Idai made landfall on 15 March 2019 (the end of the wet season in a typical year) and passed over Gorongosa (approximately 100 km inland), bringing maximum wind speeds of more than 188 km h^{-1}, torrential rains of more than 200 mm in less than 24 h, and floodwaters more than 5 m deep around Lake Urema at the centre of the park (Fig. 1 and Extended Data Fig. 2).

Some animals were unable to evade the rising floodwaters: three of eight GPS-collared bushbuck, the smallest individually monitored herbivore species, died within a week of landfall. The bushbuck that perished were smaller than the survivors (mean 35.7 kg versus 46.0 kg) and included the smallest male and smallest two females (Extended Data Fig. 3a,b). Although these three individuals began moving towards

higher and drier ground, they did not avoid the flood edge and died in areas inundated with more than 1.5 m of water (Fig. 1d and Extended Data Fig. 3c). Bushbuck sought out elevated positions at both macro-topographic scales and microtopographic scales, climbing upslope while also perching atop termite mounds—hillocks up to 5 m high and 20 m wide that became tiny islands in the flood (Fig. 2a). The path of one survivor shows how it 'hopped' from mound to mound, passing quickly through the flooded areas in between (Fig. 1d). By contrast, we did not detect any mortality among four larger species for which we had GPS location data: nyala (98 kg, $n = 4$), kudu (210 kg, $n = 12$), sable (223 kg, $n = 3$), and elephant (4,000 kg, $n = 13$). Many surviving herbivores vacated their previous ranges, moving to higher-elevation areas away from floodwaters before settling in areas of relative safety (Fig. 2b and Extended Data Fig. 4a). The degree of displacement from prior ranges was positively related to species' affiliation with low-elevation floodplain habitat and negatively correlated (albeit less strongly) with body mass (Extended Data Fig. 4b). These results are based on relatively small sample sizes of collared herbivores but provide striking real-time evidence of how different animals navigated the landscape during the storm and its aftermath, and the findings are consistent with other results below showing that small and floodplain-affiliated species were most affected by Cyclone Idai.

Data from a 300-km^2 camera-trap grid[31] (30 cameras in 5-km^2 hexagonal cells) showed that other herbivore species shifted their space use in similar ways. We found strong interactive effects of time since landfall and distance to Lake Urema on species' distributions (Extended Data Table 1), indicating that Cyclone Idai pushed herbivores out of low-lying areas and into elevated woodland, with activity near the lake declining sharply in the weeks after landfall relative to typical years (Fig. 2c). Rates of return to these areas varied. Species such as impala rebounded to pre-cyclone levels even before the flood fully subsided, whereas warthog and waterbuck (the two most floodplain-affiliated species with enough detections for analysis) remained skewed towards higher elevations into August, long after waters had receded below pre-cyclone levels (Fig. 2c).

In addition to crowding herbivores into elevated habitat, Cyclone Idai altered the spatiotemporal distribution of forage availability. The extreme and unseasonal flooding reversed the typical growth pattern of understory plants in the flood zone (Fig. 3a). Vegetation in this area remained significantly less productive than usual for three months after landfall (March to May; Fig. 3a). This effect was far less pronounced in elevated woodland areas that were not flooded after Idai (Fig. 3b). In the late dry season (October), productivity was marginally higher than in normal years, perhaps owing to atypically high soil moisture.

Cyclone-induced changes in food availability, coupled with upland shifts in distribution, altered herbivore diets. Almost all species ate a significantly different set of plant taxa throughout 2019 than in the corresponding seasons of 2016 and 2018 (Extended Data Fig. 5), and the turnover in diet composition from before to after the cyclone was significantly greater than the typical degree of between-season dietary dissimilarity (Fig. 4a). Although the nature and strength of these differences varied across species and seasons, several broad trends emerged. Post-cyclone diets tended to include less grass (especially in mixed-feeding species that characteristically eat both grasses and non-grasses; Extended Data Fig. 6a), a greater number of plant families (Extended Data Fig. 6b), and plant species that were taller (Fig. 4b) and less nutritious (lower in digestible protein, phosphorus and sodium, and higher in lignin; Figs. 4c and 5a and Extended Data Fig. 6c–f) than usual, consistent with a shift toward 'woodier' diets[32]. Dietary differences between species (that is, resource partitioning) were also stronger in the early dry season (July) of 2019 than in normal years (Fig. 4d). We propose that the depletion of understory plants and crowding of animals into high and dry areas resulted in stronger competition, pressuring herbivores to differentiate their diets and accept an
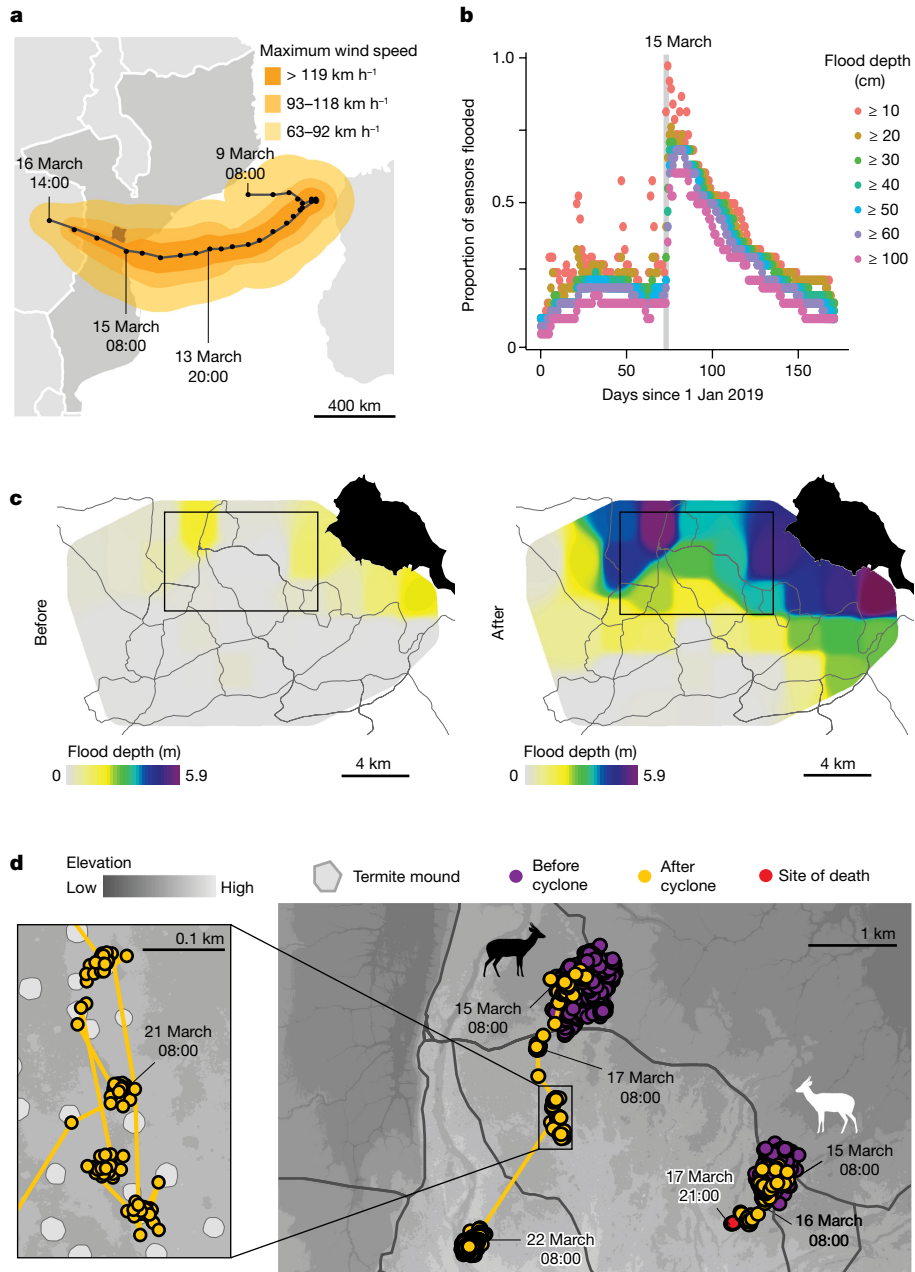
Fig. 1 | Cyclone Idai led to extensive flooding in Gorongosa. a, After making landfall on 15 March 2019, Cyclone Idai[50] (black line shows central path; dots show position every 6 h) passed over Gorongosa National Park (shaded dark grey) in central Mozambique. **b**, Heavy rains from Idai inundated a network of 37 flood sensors; flood extent did not return to pre-cyclone levels until roughly 31 May (Julian day 151 of 2019). **c**, Within a week of landfall, the flood extent (areas inundated by more than 50 cm) increased nearly fivefold (from 24.1 km² in the week before landfall to 117.7 km² in the week after; total census area, 165.8 km²) and maximum flood depth increased nearly threefold (from 2.0 m to 5.9 m). Lake Urema (top right) and roads (black lines) are shown to facilitate comparison. The rectangle shows the area of interest in **d**. **d**, Hourly GPS fixes of two bushbuck, one that survived (black silhouette) and one that died (white silhouette). Purple points show positions in the month before the cyclone; yellow points show positions in the month after the cyclone; the red point shows the site of death. The survivor left its home range and moved up the elevational gradient, away from Lake Urema, using termite mounds as refuges from the flood (enlarged image at left) before establishing a new home range approximately 3.5 km away. The individual that died started moving upslope but did not outpace the flood and died within 500 m of its original home range. This pattern was consistent across the small sample size of five bushbuck that survived and three that died (Extended Data Fig. 3).

atypically wide range of relatively low-quality forage[33]. In some cases, the cyclone effects on diet metrics were contingent on herbivore traits, with small-bodied and/or floodplain-affiliated species exhibiting higher turnover, greater increases in diet breadth, and greater reductions in dietary digestibility (Extended Data Table 2). Although these effects were not consistently significant across seasons, all significant effects were in the predicted direction.

The post-cyclone period of lower food availability and diet quality was associated with reduced nutritional condition in small-bodied antelopes. Bushbuck and nyala, the two smallest GPS-collared herbivore species (less than 100 kg), were in worse condition in 2019 than in previous years (2014–2018). The condition of kudu, a larger and wider-ranging congener with comparable dietary habits[34], was unaffected by the cyclone (Fig. 4e). Coupled with evidence of reduced diet
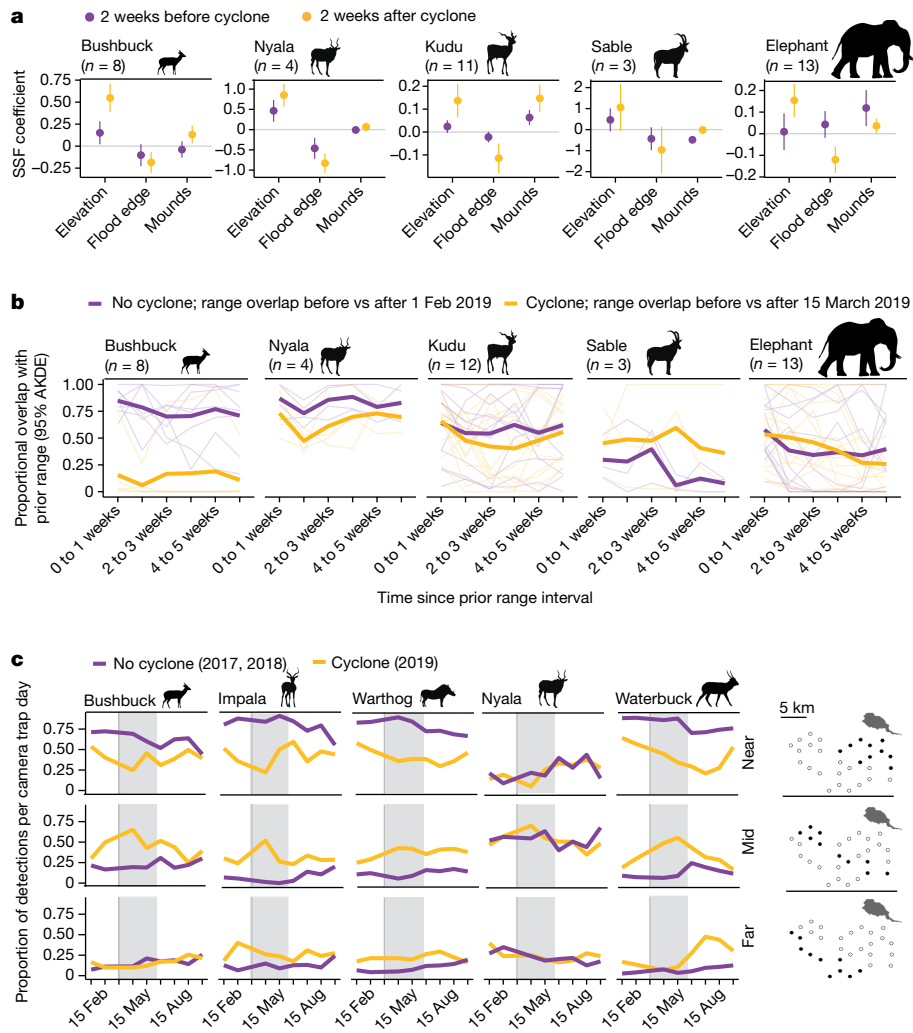
Fig. 2 | Herbivores changed their movement behaviour to avoid cyclone-induced flooding. a, Coefficients and 95% confidence intervals from step-selection functions (SSFs) for 39 GPS-collared herbivores of five species, showing the extent to which animals avoided (negative coefficients) the flood and selected (positive coefficients) higher elevations and termite mounds in the 2 weeks before (purple) and 2 weeks after (yellow) Cyclone Idai. One kudu was excluded from this analysis because its range did not overlap the extent of our environmental data. Non-overlapping confidence intervals indicate significant differences before versus after landfall. All species increased avoidance of the flood edge (significantly for kudu and elephant) and moved to higher elevations (significantly for bushbuck, kudu and—marginally—elephant). **b**, Many GPS-collared herbivores departed their previous ranges in the weeks after landfall (overlap of utilization distributions via 95% autocorrelated kernel density estimation (AKDE)), a trend not observed in non-cyclone periods (purple lines). Thin lines show individual data and bold lines show the mean.

Degree of displacement scaled negatively with species' floodplain affiliation and positively with body size (Extended Data Fig. 4b). **c**, Data from camera traps over 3 years, showing the distribution through time of five well-sampled species relative to distance from Lake Urema (that is, the proportion of total detections per species at different distances from the lake—here, binned as 'near', 'mid' and 'far' to facilitate visualization, but modelled statistically using a continuous distance term; see Extended Data Table 1) in the cyclone year (2019; yellow) versus two representative non-cyclone years (purple; average across 2017 and 2018). Binned camera locations are shown with black dots at right. Shading shows the duration that flooding persisted beyond the pre-cyclone extent (15 March–31 May). Fluctuations in slope of the yellow lines show how the cyclone displaced species away from low-lying open habitat and into higher-elevation areas away from Lake Urema, with variable rates of return in relation to flood duration.

quality after Idai, both in general (Extended Data Fig. 6) and for these species in particular (Fig. 4f), this result supports our hypothesis that larger animals were better buffered against nutritional limitation[24]. Although some studies predict that higher absolute energetic requirements might make larger herbivores more vulnerable to perturbations in food availability[35], our results align better with theory and data suggesting that larger herbivores are more resistant to nutritional limitation owing to their ability to rely on endogenous reserves and subsist on low-quality diets[36,37].

The stronger individual-level effects of Cyclone Idai on small-bodied and floodplain-associated species translated into uneven population-level impacts. From 1994 to 2018, the herbivore populations in this

study grew almost monotonically, as determined by regular aerial surveys[28]. The post-Idai survey completed in November 2020, 20 months after landfall, documented the first declines in several of these populations since the civil war (Extended Data Fig. 7). Oribi and reedbuck—two of the smallest (17–76 kg) and most floodplain-affiliated (65–81% of occurrences) species—declined by 47–53%. By contrast, 3 larger species with lower floodplain affiliation—wildebeest, buffalo and elephant (214–4,000 kg)—each increased by around 27%. In a set of 16 candidate models including main effects and interactions of body size, diet type (percentage of grass), and habitat affiliation, size alone best predicted proportional change in abundance after Cyclone Idai (R^2_{adj} = 0.28, P = 0.04, Akaike weight (AICŵ) = 0.31); habitat affiliation
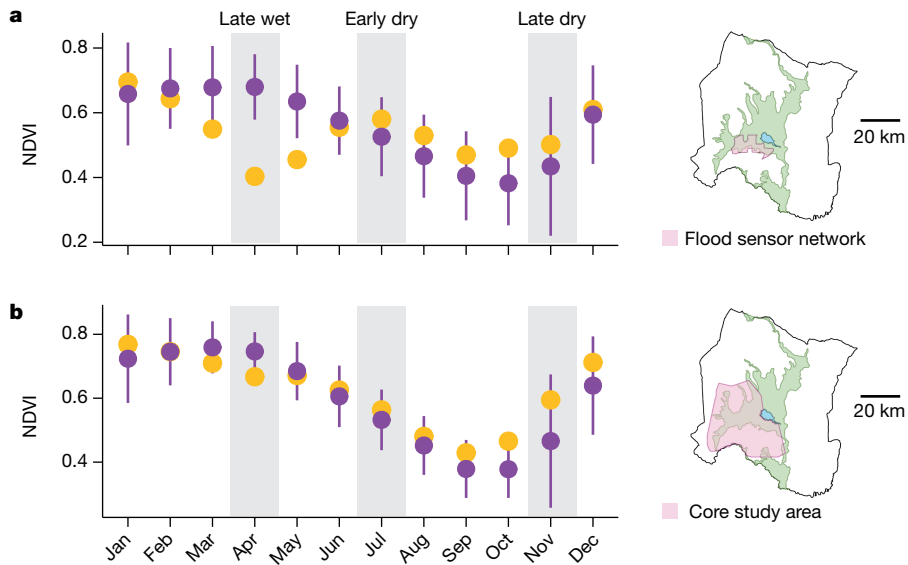
Fig. 3 | Cyclone-induced flooding depleted understory forage. Normalized difference vegetation index (NDVI), a proxy for aboveground productivity, for different focal areas in the year of Cyclone Idai (2019; yellow) compared with NDVI in those areas in 20 other years (2000–2018 and 2020; purple). Data are mean ± 2 s.d. Maps show Gorongosa National Park with floodplain habitat in green, Lake Urema in blue and the focal area for each NDVI analysis in pink. **a**, For 3 months after landfall, Cyclone Idai sharply decreased productivity in flooded portions of our study area (locations that were dry the week before Idai but under more than 0.5 m of water within 2 weeks after), as determined by our network of locally deployed sensors (March: $Z = -2.02$; April: $Z = -5.47$; May: $Z = -3.16$). NDVI was higher than usual in October 2019, although this difference ($Z = 1.67$) did not exceed the conventional threshold for statistical significance ($|Z| > 2$). **b**, These effects were muted when the focal region was expanded to the broader study area[34] (here, the 95% minimum convex polygon of location data from GPS-collared spiral-horned antelopes in 2014–2019), which includes higher-elevation habitat outside the flood zone; at this scale, NDVI differed significantly from the long-term average only in April ($Z = -2.63$). Grey bars show time periods during which we sampled herbivore diets.

alone was the second-best model and fit comparably well (difference in the Akaike information criterion (ΔAICc) = 0.96, R^2_{adj} = 0.22, P = 0.06, AICŵ = 0.19; Supplementary Table 2). These relationships did not occur in normal years: neither body mass nor habitat affiliation predicted changes in abundance from 2014–2016 or 2016–2018 (P > 0.3) (Fig. 5).

Waterbuck, a 215-kg floodplain-affiliated grazer, exemplified this trend. From 1994 to 2018, the waterbuck population grew logistically from fewer than 1,000 individuals to more than 57,000 individuals[28,37]. When the 2020 census revealed an unprecedented number of dead animals, observers conducted a systematic carcass survey, estimating at least 3,300 dead waterbuck—almost all of them in the floodplain (7.44 carcasses per km², versus 0.24 per km² in woodland). These mortalities, corresponding to roughly 6% of the 2018 population estimate and half of the difference in abundance between 2018 and 2020, contributed to the first definitive waterbuck decline (−12%) in more than 25 years.

The two large-carnivore species in Gorongosa at the time of this study exhibited behaviours consistent with a weak response to Cyclone Idai, although the available data are sparser than for herbivores. We observed no mortalities among the 22 individuals with known fates (14 wild dogs, 30 kg; 8 lions, 190 kg). The two GPS-collared lions for which we were able to fit step-selection functions moved to higher elevations and avoided the flood edge in the weeks after landfall, whereas the lone wild dog pack in the park exhibited no significant changes in movement (Extended Data Fig. 8a). Lions (n = 8) and wild dogs showed moderate displacement from their previous ranges (Extended Data Fig. 8b). We detected no change in lion diets, which were dominated by warthog both before and after the cyclone (Extended Data Fig. 8c). Wild dog diets appeared to shift in concert with prey distribution: waterbuck accounted for a greater proportion of kills after the cyclone, especially in the immediate aftermath (Extended Data Fig. 8c–e), when large numbers of waterbuck were displaced from the floodplain into wooded areas frequented by wild dogs (Fig. 2c). Lion and wild dog populations both increased from 2018 to 2020 (Extended Data Fig. 7). Analogously, carnivore populations often respond positively to drought, because hunting success increases when herbivores are weak and congregate around limited resources[38,39]. Although sample-size limitations temper our conclusions about the impacts of Cyclone Idai on carnivores, it is possible that short-term impacts of extreme weather events on large mammals vary predictably with trophic level, and future research could test this hypothesis.

Collectively, our results support trait-based hypotheses about animal robustness to tropical cyclones and show how responses propagate across spatiotemporal scales and levels of organization, from individual behaviours to population trends and community structure. Small size and affiliation with low-lying habitat were associated with lower resistance and resilience of herbivores to Cyclone Idai across timescales ranging from hours and days (reflecting differential abilities to evade rising floodwaters) to more than a year (owing to differential degrees of nutritional shortfall and ability to tolerate it). The sensitivity of these species, despite their ecological and evolutionary experience with annual flooding in Gorongosa, highlights a distinction between cyclical and unpredictable risk[40]; animals entrained by rhythmic perturbations of moderate intensity might even be especially vulnerable to unseasonal extreme events. Our study answers recent calls to investigate cyclone impacts, identify mechanisms that link ecological responses across scales, and plug geographic and taxonomic gaps in cyclone ecology[8,9]. Our findings are consistent with prior work linking body size and mobility to the robustness of small animals to cyclones on islands[6], supporting the scalability of these relationships and the proposition[7] that general trait-based models would aid in forecasting impacts of extreme events on terrestrial animals at large.

More time is needed to know whether Cyclone Idai will have lasting effects on community structure. Higher fecundity in small-bodied species might enable rapid recovery, thereby offsetting the costs of lower resistance and resilience and equalizing overall robustness[6]. Yet it is noteworthy that Idai at least transiently tipped the scale in favour of large-bodied species that predominated historically[29], perhaps signalling a tipping point in Gorongosa's postwar community reassembly (ref. 41 describes a comparable event). More broadly, our study highlights a need to consider
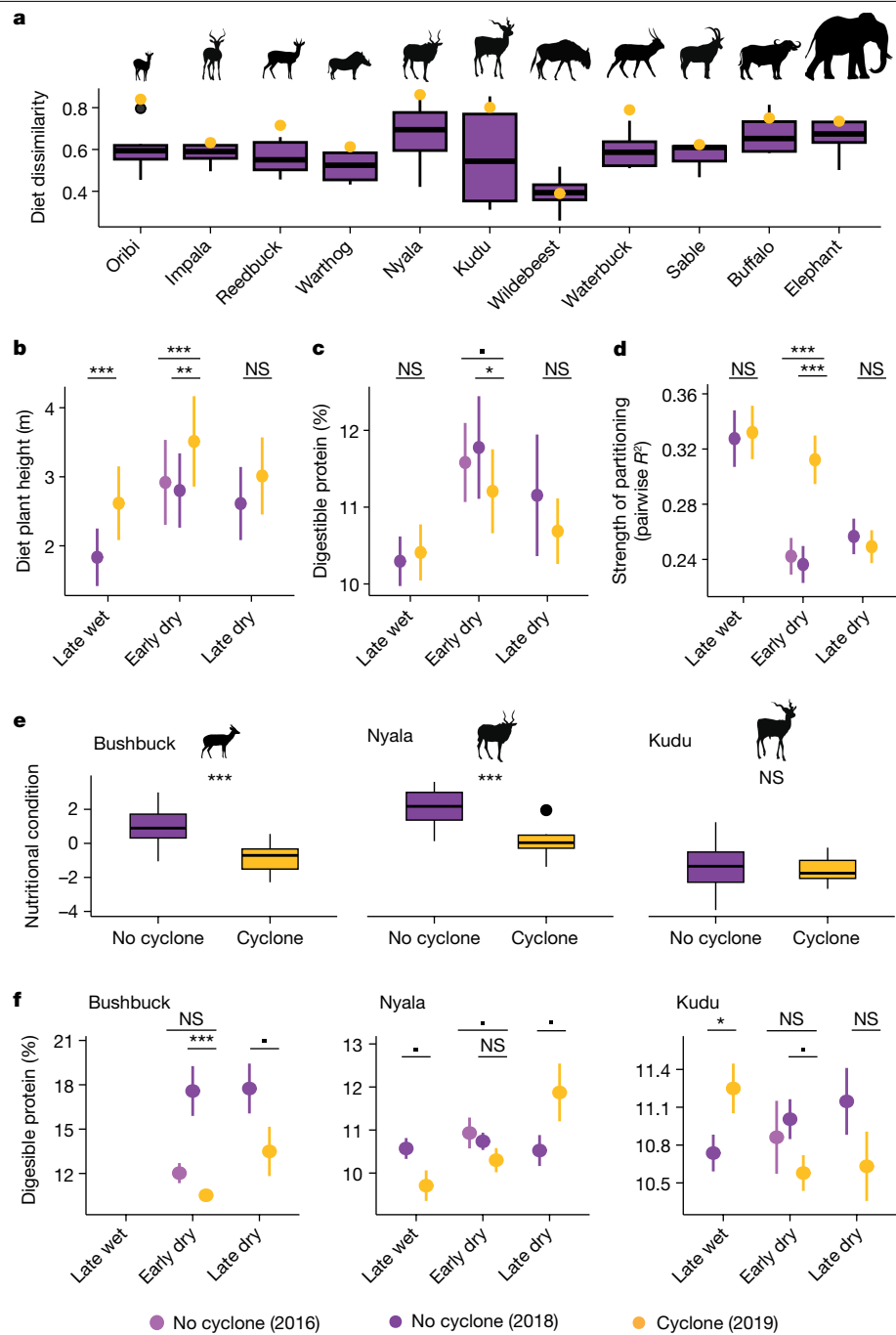
Fig. 4 | Cyclone impacts on herbivore diets and nutritional condition.
a, Temporal turnover in herbivore diets from before Cyclone Idai to after Cyclone Idai (yellow points; Bray–Curtis dissimilarity, November 2018 to April 2019) was greater than that observed within or between non-cyclone years (purple boxes; Bray–Curtis dissimilarity between all pairs of seasons in 2016 and 2018). The centre line shows the median, box edges delineate the interquartile range, whiskers extend up to 1.5× the interquartile range and dots indicate outliers. Mixed-effects model with beta error distribution across all species, $\beta = 0.53 \pm 0.16$ (mean ± s.e.m.), $P = 0.001$. **b**–**d**, On average, relative to non-cyclone years (2016 and 2018), herbivore diets after Idai comprised taller plant species (**b**; linear mixed-effects models; wet season 2018: $\beta = -0.29 \pm 0.07$; early dry season 2016: $\beta = -0.40 \pm 0.09$; early dry season 2018: $\beta = -0.25 \pm 0.08$; late dry season 2018: $\beta = -0.10 \pm 0.07$), contained less protein in the early dry season (**c**; linear mixed-effects models; wet season 2018:

$\beta = 0.02 \pm 0.17$; early dry season 2016: $\beta = -0.33 \pm 0.17$; early dry season 2018: $\beta = -0.38 \pm 0.16$; late dry season 2018: $\beta = -0.01 \pm 0.21$), and exhibited greater interspecific differentiation in the early dry season, as indexed by the mean R^2 of perMANOVA between each pair of herbivore species[33] (**d**; mixed-effects models with beta error distribution; wet season 2018: $\beta = -0.02 \pm 0.07$; early dry season 2016: $\beta = -0.37 \pm 0.04$; early dry season 2018: $\beta = -0.40 \pm 0.04$; late dry season 2018: $\beta = 0.04 \pm 0.04$). Sample sizes are presented in Supplementary Table 1. **e**, Nutritional condition of collared herbivores after Idai (2019) and in 2014–2018 (t-tests; bushbuck: $t = 6.74$, d.f. = 28.5; nyala: $t = 4.47$, d.f. = 10.2; kudu: $t = 0.61$, d.f. = 36.9). **f**, Dietary protein content for bushbuck and nyala was lower after Idai than in non-cyclone years during the period leading up to body condition measurements in **e** (mid-dry season), whereas kudu diets showed the opposite trend. Data in **b**–**d** and **f** are mean ± s.e.m. ***$P < 0.001$; **$P < 0.01$; *$P < 0.05$; ·$P < 0.10$; NS, $P > 0.10$.
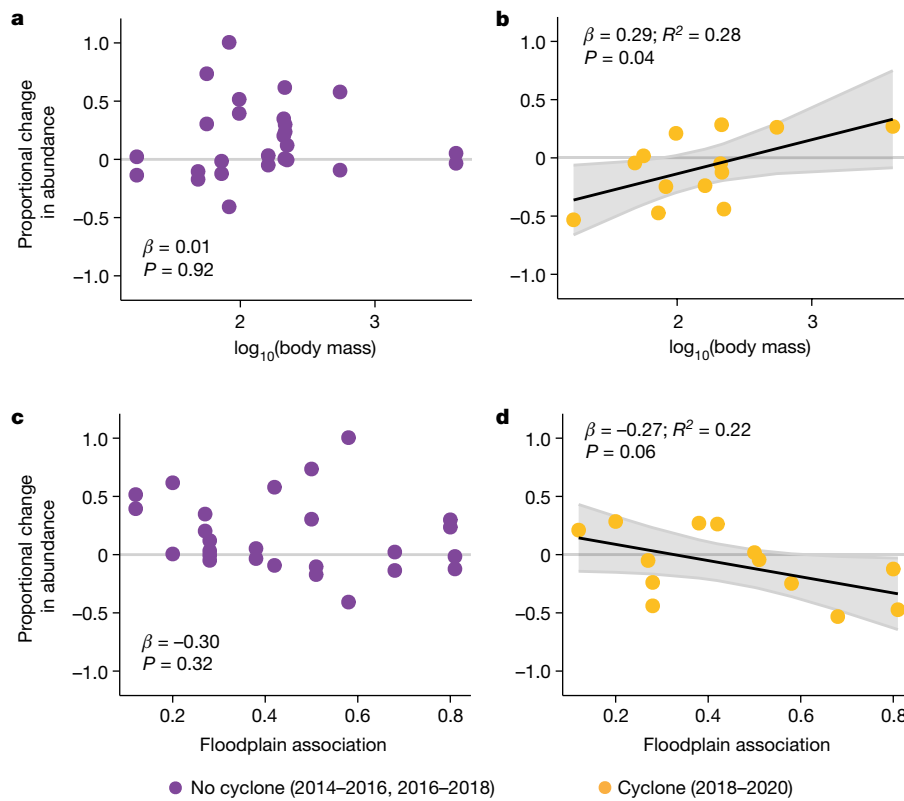
Fig. 5 | Cyclone impacts on herbivore populations varied with body size and habitat affiliation. a–d, Proportional change in abundance between October 2018 and November 2020 (**b,d**) was positively correlated with herbivore body size (**b**), with smaller species exhibiting greater declines, and was negatively correlated with affinity for low-elevation grassland habitat (**d**), with floodplain-affiliated species exhibiting greater declines. These two traits were uncorrelated with each other (Extended Data Fig. 1a) and did not predict changes in abundance between normal years (2014–2016 and 2016–2018), either when considered together (**a,c**) or analysed separately ($P > 0.45$ for each trait in regressions for 2014–2016 and 2016–2018, independently).

natural hazards in rewilding, which is advocated in part to buffer ecosystems against disturbance but will also be influenced by such disturbances[1,42]. Traits conferring fast population growth (small size) may accelerate restoration but at the cost of vulnerability to storms; conversely, very large megaherbivores such as elephants are integral to ecosystem function[5] and relatively robust to floods (this study) but may be more sensitive to heatwaves[35]. Analysing impacts of extreme events as continuous functions of their intensity against the backdrop of shifting climatic baselines in ecosystems worldwide—rather than as isolated events at particular locations—is an important next step for the field[8,9] and is increasingly feasible with globally distributed wildlife monitoring[43,44].

As severe weather intensifies in concert with other threats to biodiversity, a better understanding of how perturbations affect population persistence and ecosystem integrity is a pressing goal[1,43]. By identifying correlates of robustness to cyclones among disproportionately threatened megafauna[5,45], our study contributes to ongoing discussions about potential adaptation measures and interventions to mitigate impacts on species of concern[1]. Proactively identifying vulnerable habitats and populations before extreme events occur will help managers devise and implement strategies—for example, driving animals away from at-risk areas before storms hit[46,47] or providing supplemental food afterwards[48,49]—to reduce undesired ecological impacts of climatic volatility.

Online content

Any methods, additional references, Nature Portfolio reporting summaries, source data, extended data, supplementary information, acknowledgements, peer review information; details of author contributions and competing interests; and statements of data and code availability are available at https://doi.org/10.1038/s41586-023-06722-0.

1.   IPCC. *Climate Change 2022: Impacts, Adaptation and Vulnerability* (eds Pörtner, H.-O. et al.) (Cambridge Univ. Press, 2022).
2.   Smith, M. An ecological perspective on extreme climatic events: a synthetic definition and framework to guide future research. *J. Ecol.* **99**, 656–663 (2011).
3.   Ummenhofer, C. C. & Meehl, G. A. Extreme weather and climate events with ecological relevance: a review. *Phil. Trans. R. Soc. B* **372**, 20160135 (2017).
4.   Jentsch, A., Kreyling, J. & Beierkuhnlein, C. A new generation of climate-change experiments: events, not trends. *Front. Ecol. Environ.* **5**, 365–374 (2007).
5.   Pringle, R. M. et al. Impacts of large herbivores on terrestrial ecosystems. *Curr. Biol.* **33**, R584–R610 (2023).
6.   Spiller, D. A., Losos, J. B. & Schoener, T. W. Impact of a catastrophic hurricane on island populations. *Science* **281**, 695–697 (1998).
7.   Schoener, T. W. & Spiller, D. A. Nonsynchronous recovery of community characteristics in island spiders after a catastrophic hurricane. *Proc. Natl Acad. Sci. USA* **103**, 2220–2225 (2006).
8.   Pruitt, J. N., Little, A. G., Majumdar, S. J., Schoener, T. W. & Fisher, D. N. Call-to-Action: a global consortium for tropical cyclone ecology. *Trends Ecol. Evol.* **34**, 588–590 (2019).
9.   Lin, T. C., Hogan, J. A. & Chang, C. T. Tropical cyclone ecology: a scale-link perspective. *Trends Ecol. Evol.* **35**, 594–604 (2020).
10. IPCC. *Climate Change 2021: The Physical Science Basis* (eds Masson-Delmotte, V. et al.) (Cambridge Univ. Press, 2021).
11. Knutson, T. R. et al. in *Critical Issues in Climate Change Science* (eds Quéré, C. L. et al.) (ScienceBrief, 2021).
12. Guzman, O. & Jiang, H. Global increase in tropical cyclone rain rate. *Nat. Commun.* **12**, 5344 (2021).
13. Wang, G., Wu, L., Mei, W. & Xie, S. P. Ocean currents show global intensification of weak tropical cyclones. *Nature* **611**, 496–500 (2022).
14. Zeng, H., Chambers, J. O., Negrón-Juárez, R. I. & Powell, M. D. Impacts of tropical cyclones on US forest tree mortality and carbon flux from 1851 to 2000. *Proc. Natl Acad. Sci. USA* **106**, 7888–7892 (2009).
15. Tanner, E. V., Rodriguez-Sanchez, F., Healey, J. R., Holdway, R. J. & Bellingham, P. J. Long-term hurricane damage effects on tropical forest tree growth and mortality. *Ecology* **95**, 2974–2983 (2014).
16. Wiley, J. W. & Wunderle, J. M. Jr The effects of hurricanes on birds, with special reference to Caribbean islands. *Bird Conserv. Int.* **3**, 319–349 (1993).

17. Schoener, T. W., Spiller, D. A. & Losos, J. B. Variable ecological effects of hurricanes: the importance of seasonal timing for survival of lizards on Bahamian islands. *Proc. Natl Acad. Sci. USA* **101**, 177–181 (2004).

18. Grant, P. R. et al. Evolution caused by extreme events. *Proc. R. Soc. B* **372**, 20160146 (2017).

19. Donihue, C. M. et al. Hurricane-induced selection on the morphology of an island lizard. *Nature* **560**, 88–91 (2018).

20. Noonan, M. J. et al. Effects of body size on estimation of mammalian area requirements. *Conserv. Biol.* **34**, 1017–1028 (2020).

21. Bowman, J., Jaeger, J. A. G. & Fahrig, L. Dispersal distance of mammals is proportional to home range size. *Ecology* **83**, 2049–2055 (2002).

22. Loe, L. E. et al. Behavioral buffering of extreme weather events in a high-Arctic herbivore. *Ecosphere* **7**, e01374 (2016).

23. Abernathy, H. N. et al. Deer movement and resource selection during Hurricane Irma: implications for extreme climatic events and wildlife. *Proc. R. Soc. B* **286**, 20192230 (2019).

24. Peters, R. H. *The Ecological Implications of Body Size* (Cambridge Univ. Press, 1983).

25. Millar, J. S. & Hickling, G. J. Fasting endurance and the evolution of mammalian body size. *Funct. Ecol.* **4**, 5–12 (1990).

26. Warren, M. Why Cyclone Idai is one of the Southern Hemisphere's most devastating storms. *Nature* https://doi.org/10.1038/d41586-019-00981-6 (2019).

27. Charrua, A. B., Padmanaban, R., Cabral, P., Bandeira, S. & Romeiras, M. M. Impacts of the tropical Cyclone Idai in Mozambique: a multi-temporal Landsat satellite imagery analysis. *Remot. Sens.* **13**, 201 (2021).

28. Stalmans, M. E., Massad, T. J., Peel, M. J. S., Tarnita, C. E. & Pringle, R. M. War-induced collapse and asymmetric recovery of large-mammal populations in Gorongosa National Park, Mozambique. *PLoS ONE* **14**, e0212864 (2019).

29. Tinley, K. L. *Framework of the Gorongosa Ecosystem*. DSc thesis, University of Pretoria (1977).

30. Böhme, B., Steinbruch, F., Gloaguen, R., Heilmeier, H. & Merkel, B. Geomorphology, hydrology, and ecology of Lake Urema, central Mozambique, with a focus on lake extent changes. *Phys. Chem. Earth.* **31**, 745–752 (2006).

31. Gaynor, K. M., Daskin, J. H., Rich, L. N. & Brashares, J. S. Post-war wildlife recovery in an African savanna: evaluating patterns and drivers of species occupancy and richness. *Anim. Conserv.* **24**, 510–522 (2021).

32. Potter, A. B. et al. Mechanisms of dietary resource partitioning in large-herbivore assemblages: a plant-trait-based approach. *J. Ecol.* **110**, 817–832 (2022).

33. Pansu, J. et al. Generality of cryptic dietary niche differentiation in diverse large-herbivore assemblages. *Proc. Natl Acad. Sci. USA* **119**, e2204400119 (2022).

34. Daskin, J. H. et al. Allometry of behavior and niche differentiation among congeneric African antelopes. *Ecol. Monogr.* **93**, e1549 (2022).

35. Veldhuis, M. P. et al. Large herbivore assemblages in a changing climate: incorporating water dependence and thermoregulation. *Ecol. Lett.* **22**, 1536–1546 (2019).

36. Abraham, J. O., Hempson, G. P. & Staver, A. C. Drought-response strategies of savanna herbivores. *Ecol. Evol.* **9**, 7047–7056 (2019).

37. Becker, J. A. et al. Ecological and behavioral mechanisms of density-dependent habitat expansion in a recovering African ungulate population. *Ecol. Monogr.* **91**, e01476 (2021).

38. Loveridge, A. J., Hunt, J. E., Murindagomo, F. & Macdonald, D. W. Influence of drought on predation of elephant (*Loxodonta africana*) calves by lions (*Panthera leo*) in an African wooded savannah. *J. Zool.* **270**, 523–530 (2006).

39. Ferreira, S. M. & Viljoen, P. African large carnivore population changes in response to a drought. *Afr. J. Wildl. Res.* **52**, 1 (2022).

40. Palmer, M. S. et al. Dynamic landscapes of fear: understanding spatiotemporal risk. *Trends Ecol. Evol.* **37**, 911–925 (2022).

41. Thibault, K. & Brown, J. Impact of an extreme climatic event on community assembly. *Proc. Natl Acad. Sci. USA* **105**, 3410–3415 (2008).

42. Perino, A. et al. Rewilding complex ecosystems. *Science* **364**, eaav5570 (2019).

43. Betts, M. G. et al. Extinction filters mediate the global effects of habitat fragmentation on animals. *Science* **366**, 1236–1239 (2019).

44. Tucker, M. A. et al. Behavioral responses of terrestrial mammals to COVID-19 lockdowns. *Science* **380**, 1059–1064 (2023).

45. Ripple, W. J. et al. Status and ecological effects of the world's largest carnivores. *Science* **343**, 1241484 (2014).

46. Meagher, M. Evaluation of boundary control for bison of Yellowstone National Park. *Wildl. Soc. Bull.* **17**, 15–19 (1989).

47. Laubscher, L. L. et al. Non-chemical techniques used for the capture and relocation of wildlife in South Africa. *Afr. J. Wildl. Res.* **45**, 275–286 (2015).

48. Walker, B. H., Emslie, R. H., Owen-Smith, N. & Scholes, R. J. To cull or not to cull: lessons from a southern African drought. *J. Appl. Ecol.* **24**, 381–401 (1987).

49. Milner, J. M., van Beest, F. M., Brook, R. K. & Storaas, T. To feed or not to feed? Evidence of the intended and unintended effects of feeding wild ungulates. *J. Wildl. Manage.* **78**, 1322–1334 (2014).

50. Joint Research Centre. *Tropical Cyclone IDAI in Mozambique (2019-03-15)*. http://data.europa.eu/89h/4f8c752b-3440-4e61-a48d-4d1d9311abfa (European Commission, 2019).

Methods

Study system

Gorongosa National Park is located at the southern tip of the Great Rift Valley (−18.96° N, 34.36° E) approximately 100 km from the Mozambique Channel (Fig. 1a). The Great Rift Valley runs through the park and encompasses Lake Urema, a large (dry season extent ≈ 18 km²), shallow (dry season depth ≈ 1.5 m) waterbody fed by multiple rivers in the 9,300-km² catchment[29]. Most rainfall (mean 850 mm, interquartile range 650–1,080 mm from 1957 to 2018) occurs during a wet season from November–April; then, Lake Urema expands, flooding up to 780 km² of the Rift floor[29,30]. Floodwaters recede as the dry season progresses (May–October), and Lake Urema persists as a perennial water source. Our study area lies south and west of Lake Urema, where vegetation structure and hydrology distinguish three habitat types: (1) floodplain grassland (8–20 m elevation), an annually flooded, productive zone of grasses and forbs that supports a large portion of Gorongosa's wildlife; (2) floodplain–savanna transition (20–25 m elevation), which occasionally floods and features patchy stands of water-tolerant trees such as fever tree (*Vachellia xanthophoea*), white acacia (*Faidherbia albida*) and palms (*Hyphaene* spp.); and (3) savanna woodland (> 25 m elevation), which rarely floods and supports diverse tree species and a full continuum of canopy cover (Extended Data Fig. 1b–e)[33,37,51–54].

Gorongosa historically supported big herds of large-bodied (>200-kg) grazers such as hippopotamus (*Hippopotamus amphibius*), buffalo (*Syncerus caffer*), wildebeest (*Connochaetes taurinus*) and zebra (*Equus quagga*), along with substantial populations of large carnivores, including lion (*Panthera leo*), leopard (*Panthera pardus*) and African wild dog (*Lycaon pictus*)[28]. During and after the 1977–1992 Mozambican Civil War—when intense fighting occurred in Gorongosa—all large-mammal populations declined by >90% and leopard and wild dog were extirpated[28]. By 2018, restoration efforts had helped to recover total herbivore biomass to >90% of pre-war estimates, including all of the ungulate species present in 1972. Lion abundance rebounded to at least 50% of the estimated historical population size of 200 by 2016 and has continued to increase, although the exact population size in 2019 is unknown[28,55]. A founding pack of 14 wild dogs was reintroduced in June 2018, shortly before Cyclone Idai[56]; leopard and hyena were not reintroduced until 2020 and 2022, respectively. Gorongosa's megafauna was thus largely intact in terms of species composition at the time of our study, but community structure was shifted relative to the pre-war baseline in favour of smaller species (≤200 kg). Waterbuck (*Kobus ellipsiprymnus*), reedbuck (*Redunca arundinum*), warthog (*Phacochoerus africanus*), impala (*Aepyceros melampus*) and oribi (*Ourebia ourebi*) collectively accounted for 67% of biomass in 2018, whereas the formerly dominant large-bodied species remained rare[28].

From 1980 to 2007, an average of 1.2 cyclones per year made landfall in Mozambique[57,58]. However, Idai (a category 4-equivalent intense tropical cyclone), which made landfall at the port city of Beira on 15 March 2019, is by some measures the worst cyclone on record in the Southern hemisphere[26,27]. Idai caused widespread damage throughout Mozambique, Zimbabwe and Malawi, resulting in more than US$3.2 billion in damage and more than 1,600 deaths[26,59]. In Gorongosa, >200 mm of rain fell in 24 h (nearly a quarter of the annual mean), and estimated sustained winds in the park exceeded 93 km h⁻¹ (ref. 50).

We integrated data from multiple, concurrent research projects to capture individual and population-level responses of the two extant large carnivores (lion and wild dog)[55,56] and the 13 most abundant (>500 counted in 2018) large-herbivore species[28]: elephant (*Loxodonta africana*), buffalo, sable (*Hippotragus niger*), wildebeest, waterbuck, kudu (*Tragelaphus strepsiceros*), hartebeest (*Alcelaphus buselaphus*), nyala (*Tragelaphus angasii*), warthog, reedbuck, impala, bushbuck (*Tragelaphus sylvaticus*) and oribi. Six herbivore species were not included because they were too scarce (<200 counted in 2018: zebra, eland, bushpig, and grey and red duiker) and/or limited to a narrow range of habitats outside our core study area (hippopotamus and duikers). The study species span two orders of magnitude in body mass[60] and a range of habitat associations (Extended Data Fig. 1): herbivore floodplain affiliation ranged 12–81%, quantified as the mean proportion of individuals occurring in treeless floodplain grassland[37,54] during biennial wildlife counts from 2014–2018 (see 'Aerial wildlife surveys'). Data were not available for all species in every analysis. Movement data were available for elephant, sable, kudu, nyala, bushbuck, lion and wild dog; camera traps produced adequate sample sizes for waterbuck, nyala, warthog, impala and bushbuck; and nutritional condition data were available for kudu, nyala and bushbuck. Diet and abundance data were available for all species.

Quantifying flood depth and extent

We tracked flood depth throughout the park's road network before and after Cyclone Idai using loggers deployed in 2018. From August to November 2018, we installed 46 automated water-level loggers (HOBO U20L-01, Onset) in a regular grid with 1.8-km spacing between locations, covering a 120-km² minimum convex polygon. An additional logger was deployed indoors at the park's research headquarters to record atmospheric pressure, which we later used to correct raw pressure readings from the other sensors (that is, to obtain pressure of water independent of air pressure).

All sensors were set to record water levels every 4 h and were deployed inside slotted PVC pipes set vertically into the ground and capped with PVC to reduce disturbance by wildlife; pipes were tied with stainless steel to metal stakes driven 60–100 cm into the ground. We measured depth from ground level to the bottom of each hole in which sensors were deployed.

From June to September 2019, as floodwaters receded and sites became accessible, we retrieved logger data. Of 46 loggers deployed, 37 had intact data that were included in our analyses. We truncated data from 16 November 2018 at 04:00 to 21 June 2019 at 08:00. For each sensor, we subtracted atmospheric pressure from raw recorded pressure to obtain water pressure. This enabled us to calculate water depths at each location using HOBOWare and its Barometric Compensation Assistant tool. We further corrected each estimate by subtracting the hole depth for each sensor to obtain depth above ground level.

We used an inverse distance weighting function to interpolate water depth (30-m resolution) from the corrected measurements across the minimum convex polygon encompassing all 46 original loggers, plus a 1-km buffer. We interpolated water depths in R using function idw in the package gstat[61,62]. In the absence of extensive validation data (for example, manually measured depths), we considered it best to use a relatively simple interpolation method as opposed to, for example, kriging. We used a high power (p = 7) to weight interpolated water levels toward values at the nearest measured water depth, because all else equal, closer locations should have more similar water depths. When we tested the interpolation using lower powers (p = 3 and p = 5), the influence of distant sensors led to unrealistic spotting patterns.

The flood sensor network did not fully overlap the extent of GPS collar data. Accordingly, for analyses of behavioural responses to the flood edge, we used publicly available geospatial data on flooding after Cyclone Idai from the UN Operational Satellite Applications Programme (surface waters in the central provinces of Mozambique, at 10-m resolution, derived from Sentinel-1 imagery acquired 13–26 March 2019)[63].

NDVI analysis

To evaluate how the increased extent and duration of flooding after Cyclone Idai impacted vegetation productivity, and hence availability of green forage for herbivores, we compared trends in mean monthly normalized difference vegetation index (NDVI) from 2019 with those from 20 bracketing years (2000–2018 and 2020). NDVI measures greenness; low values (approaching 0) indicate low aboveground primary productivity, high values (approaching 1) indicate high productivity[64].

Article

We analysed how NDVI in 2019 differed from other years both within the area of cyclone-induced flooding inferred from the local flood sensor data and within a more-encompassing 748-km² polygon defined by the movements of GPS-collared antelopes in 2014–2019 that included adjacent higher-elevation savanna woodland habitat[34].

We calculated NDVI from MODIS data downloaded using the MODIStsp package[65] in R and extracted monthly 1-km vegetation index products (MOD13A and MYD13A3) with NDVI, quality, usefulness, and land/water bands from February 2000 to December 2020 (MYD13A3 products are available only from July 2002). We restricted spatial extent to the two focal areas described above. We retained only pixels with quality labels of 0 or 1 (unobscured pixels), usefulness labels of <3 (highest quality) and land labels of 1 (pixel values did not represent water); other pixels were assigned 'NA'. To generate one NDVI estimate per pixel per month, we averaged values from MOD13A and MYD13A3 when both were available. For each focal area, we calculated mean monthly NDVI across pixels. We compared NDVI in each month of 2019 to the inter-annual mean and standard deviation from 2000–2018 and 2020 (Fig. 3) by computing the anomaly (Z score) for each month; $|Z| > 2$ indicates that NDVI in 2019 was >2 s.d. from the long-term mean and is a common threshold used for inferring statistical significance[66].

Animal movement analysis

We used data from GPS-collared bushbuck ($n = 8$), nyala ($n = 4$), kudu ($n = 12$), sable ($n = 3$), elephant ($n = 13$), wild dog ($n = 1$ pack) and lion ($n = 8$) collected as part of long-term studies[34,54–56,67–69]. In the lone pack of wild dogs, the dominant female was fitted with a GPS collar; because wild dogs are an obligately social species that live and hunt communally and there were no other packs in the park during our study, we considered the movement data from this female to represent the entire wild dog population in Gorongosa[56]. We limited herbivore and lion GPS data to individuals in separate herds or prides, to ensure that movements were independent. For all species, GPS collars were deployed only on animals judged to be full-grown adults based on body size, pelage, horn growth and/or tooth wear. We measured body weights of bushbuck and female nyala by weighing them during immobilization for collaring. Male nyala, along with kudu and sable of both sexes, are too large to easily weigh in the field; we used chest girth measurements for these individuals to estimate body mass based on regressions developed for antelopes in Gorongosa[34]. Chest girth was not measured for elephant; we thus assumed all individual weights to be the average of sex-specific adult body mass estimates[60] (as we did for all non-collared species; Extended Data Fig. 1). Animal-handling procedures followed guidelines established by the American Society of Mammalogists[70]. Bushbuck, nyala and kudu protocols were approved by Animal Care and Use Committees at the University of Idaho (2019-32) and Princeton University (2075F-16). Sable protocols were approved by the animal ethics committee at the University of Witwatersrand (2013/47/2 A). Elephant protocols were approved by the Animal Care and Use Committee at the University of Idaho (2015-39) and Gorongosa National Park's Conservation Department. Lion and wild dog protocols were approved by the Gorongosa Conservation Department.

We evaluated how distance to floodwaters, elevation, and proximity to termite mounds influenced movements of GPS-collared animals during the first two weeks after the onset of flooding (that is, 04:00 15 March 2019, the hour at which >10% of flood sensors detected an increase in depth) using step-selection functions (SSFs)[71,72]. Mounds created by fungus-farming *Macrotermes* spp.—substantial hills that can grow to >5 m tall and >20 m diameter—are ubiquitous in the wooded portions of our study area and are selected by browsing antelopes owing to their dense and nutrient-rich woody plants[34,73]. To test our predictions that animals would avoid the flood edge and move to high ground at both coarse and fine spatial grains (higher-elevation areas and termite mounds within those areas), we fit separate SSFs for each species for two-week intervals before (04:00 1 March to 04:00 15 March

2019) and after (04:00 15 March to 04:00 29 March 2019) Idai. We paired each observed time step (segments linking consecutive relocations, which occurred at 1-h intervals for bushbuck, nyala, kudu and elephant; 3-h intervals for lion and wild dog; and 8-h intervals for sable) with 10 random steps drawn from the distribution of step lengths and turning angles observed for each individual. For each 'used' (actual) and 'available' (random) step, we extracted: (1) distance to flood edge (m) estimated from satellite-derived shapefiles[63]; (2) elevation (m above sea level) from a LiDAR digital terrain model (0.5 m horizontal, 0.1 m vertical resolution; details in ref. 34); and (3) presence or absence of a termite mound (manually digitized in a hillshade rendering of the LiDAR-derived digital terrain model and buffered by 10 m to account for error in GPS collar fixes[34]). We limited observed and random steps to the extent of the LiDAR-derived products from which we extracted environmental covariates; one collared kudu was excluded from SSF analysis because its home range did not overlap the environmental covariates. Only two of the eight lion GPS collars collected data at sufficiently regular intervals in the weeks before and after Idai to be valid for SSF analysis. We standardized all predictor variables by subtracting the mean from each observation and dividing by the s.d. We compared standardized environmental covariate values between used and available steps in each time interval, clustered by individual, using conditional logistic regression in the survival package in R[72,74,75]. We considered differences in selection between 'before' and 'after' cyclone windows to be statistically significant when the 95% confidence intervals around their coefficients did not overlap. Inferences about cyclone impacts on movement are based on within-species comparisons of selection before versus after Idai landfall, because differing fix rates limit comparability of movement behaviour among species.

To assess whether the three bushbuck that died within a week of landfall exhibited different patterns of habitat selection than the five that survived until their collars were remotely released in May 2019, we filtered GPS data to include only the week before (04:00 8 March to 04:00 15 March 2019) and after landfall (04:00 15 March to 04:00 22 March 2019). We fit separate SSFs to the data from each period for the group that survived and the group that died (Extended Data Fig. 3c). SSF fitting procedures and statistical inference were as described above.

To evaluate the extent to which collared individuals were displaced from their prior ranges by Cyclone Idai, we partitioned individuals' GPS locations into temporal bins spanning: (1) the week before the cyclone (04:00 8 March to 04:00 15 March 2019); and (2) 6 weekly bins after flooding began. We then calculated: (1) distance between the centroid of movement (geographic mean of GPS fixes) in the week before Idai and the centroids of movement in each week thereafter; and (2) proportional overlap between the individual's range in the week before Idai (derived from 95% utilization distributions via autocorrelated kernel density estimation) and each weekly range in the 6 weeks afterwards. We calculated autocorrelated kernel density estimates for each partitioned dataset conditional on the continuous-time movement model that best fit the data (Brownian motion, Orstein–Uhlenbeck process, or Orstein–Uhlenbeck foraging process), using model selection based on the Akaike information criterion (AICc) (fit_ctmm and hr_adke in the amt package[76–78]). To test if post-cyclone displacement differed from normal patterns, we compared GPS data from representative non-cyclone time periods partitioned into a week-long 'before' range (04:00 25 January to 04:00 1 February 2019) with 6 weekly 'after' ranges (Fig. 2b and Extended Data Figs. 4a and 6b). We used Welch's two-sample t-tests to compare displacement for each species between the before-cyclone and each after-cyclone period. We assessed sensitivity of our results to the temporal partitioning of GPS data by rerunning analyses for bushbuck (the species with the greatest post-cyclone displacement and the most pre-cyclone GPS data) with different specifications, which indicated that our inferences about displacement were robust to duration of the 'before' interval (1 week to 3 months) and choice of the period used to define 'typical' movement (earlier in 2019

versus the same time of year in 2015 and 2020) (Welch's two-sample *t*-test: all $t > -3.2$, all $P < 0.02$).

We tested the roles of body size (log-transformed to meet model assumptions) and habitat affiliation (Extended Data Fig. 1a) in predicting displacement using generalized linear mixed-effects models (GLMMs) with a beta error distribution (for proportional response variables bounded by 0 and 1) and per-species random intercepts (Extended Data Fig. 4b). We fit GLMMs in glmmTMB[79] and inspected residuals using simulateResiduals() in DHARMa[80], finding no evidence that model assumptions were violated.

Camera-trap analysis

To evaluate cyclone effects on herbivore spatiotemporal distribution, we used data from a camera-trap grid established in 2016[31]. Cameras (Bushnell TrophyCam) were deployed over a 300-km^2 area south of Lake Urema, centred within 5-km^2 hexagonal cells (each camera ~2.4 km from 6 nearest neighbours)[31]. Of 48 cameras deployed at the time of landfall, 30 survived (Fig. 2c). We limited analyses to data from these 30 cameras in all years (2017, 2018 and 2019) to avoid biases arising from unbalanced sampling among cameras/years. We thinned data to >15 min between records to minimize bias arising from successive sightings of the same individuals[31]. We summed remaining detections into month-long bins from 15 March to 15 October in each year. Five species—waterbuck, nyala, warthog, impala, and bushbuck—had enough data for statistical analysis ($n > 10$ per monthly bin after 15 March in each year).

For each species, we fit a GLMM with negative-binomial distribution to model number of detections per month at each camera, offset by the log-transformed number of days per month each camera was active (to account for search effort) and the total number of detections across the grid per month (to account for variable abundance among years). This analysis tested for differences in spatiotemporal distribution between cyclone and non-cyclone years (a categorical main effect) and whether such differences were modulated by the continuous variables of months since landfall and distance from Lake Urema (cyclone × month, cyclone × lake, and cyclone × lake × month interactions). Negative three-way interaction terms indicated that herbivore activity was lower at locations closer to the lake after Idai than in normal years, and that this effect varied with time since landfall (Extended Data Table 1). We included camera and year as random intercepts to account for unmeasured variation among camera locations and between non-cyclone years. All analyses used glmmTMB and DHARMa as described above.

Carnivore diets

We partitioned previously published observations[56] of lion and wild dog kills in Gorongosa from 2017–2020 into three periods—before cyclone, 1–3 months after landfall, and 4–9 months after landfall—to explore changes in prey composition (Extended Data Fig. 8c). We used DNA metabarcoding of wild dog scats to cross-check cyclone-induced dietary shifts suggested by the kill data (Extended Data Fig. 8d,e). Scats were collected opportunistically between June 2018 and December 2019 ($n = 102$). Details of DNA extraction, amplification and sequencing are in Supplementary Methods. In brief, DNA was extracted in batches of 29 samples and 1 negative control (750 µl DNA lysis buffer). Extracted DNA from wild dog scats was loaded onto two 96-well plates for amplification. We used established primers targeting the mitochondrial 16S gene to amplify mammalian DNA[81]. We pooled PCR products by plate and purified them with a Qiagen MinElute PCR Purification kit. Purified PCR products were submitted for sequencing as equimolar libraries to the genomics core facility at Princeton University, where Illumina tags were appended with a low-cycle PCR approach and libraries sequenced in paired-end (2×150 bp) on a NovaSeq SP 300-nt platform.

Sequence data were curated and filtered using OBITools[82]. The filtered dataset comprised 87 wild dog samples and 17 prey sequences. To make samples comparable, we rarefied them to 1,000 reads, iterated

1,000 times, and used the mean relative read abundance (RRA) of prey sequences across the ensemble to represent each sample's composition. To avoid pseudoreplication, we combined samples collected on the same date, as multiple scats were often collected from the same locale on the same day. We averaged the composition of these samples, yielding $n = 42$, which we split into three periods: before cyclone (24 June to 5 December 2018, $n = 23$); 1 to 3 months after landfall (7 April to 9 June 2019, $n = 5$); and 4 to 9 months after landfall (16 July to 14 December 2019, $n = 14$). We tested for an overall compositional difference among these periods and between each pair of periods separately using adonis2 in vegan[83]. We visualized results using non-metric multidimensional scaling of Bray–Curtis dissimilarities (metaMDS in vegan). One outlier (96% of RRA identified as civet (*Civetticis civetta*)) was excluded from analysis because it may have been civet faeces mistakenly labelled as wild dog scat. Adjusting the post-cyclone temporal binning to balance sample sizes (that is, 7 April to 30 July 2019, $n = 9$; 3 August to 14 December 2019, $n = 10$) did not qualitatively alter the results. Accordingly, we present data from the June–July split that distinguishes the earliest post-cyclone period and corresponds with a natural break in sampling.

Herbivore diet composition

We used DNA metabarcoding to characterize herbivore diets, following protocols from our prior work in Gorongosa[32–34,37,51,53,54,69,84] and largely as described above for carnivores; details and subtle differences between carnivore and herbivore pipelines are in Supplementary Methods. We analysed samples collected before (2016 and 2018) and after (2019) the cyclone in three seasons: late wet season (April–May), early dry season (June–July, 2016 only), and late dry season (October–November). Raw data are on Dryad Digital Archive (2016, https://doi.org/10.5061/dryad.63tj806; 2018, https://doi.org/10.5061/dryad.sxksn02zc; and 2019, https://doi.org/10.5061/dryad.7wm37pvzv). The dataset comprised 13 herbivore species, 1,470 samples, and 332 plant molecular operational taxonomic units (mOTUs; Supplementary Table 1).

To evaluate cyclone impacts on herbivore diet composition relative to non-cyclone years, we calculated, for each species and season, Bray–Curtis dissimilarity between each pair of faecal samples from 2016 and 2018 (non-cyclone) and 2019 (cyclone). We visualized differences between years (within seasons) using non-metric multidimensional scaling and tested for significant differences using permutational multivariate analysis of variance (perMANOVA; Extended Data Fig. 5). We plotted data from 2016 and 2018 separately for visualization but lumped them into a 'non-cyclone' category for perMANOVA.

To test whether Cyclone Idai influenced temporal dietary turnover between seasons, we computed first the population-level average diet of each species (mean RRA of each mOTU across samples) and then Bray–Curtis dissimilarity (vegdist in vegan) between late dry season 2018 and late wet season 2019 (the sampling periods immediately before and after Idai). We compared that value with those obtained for all other pairs of seasons (both consecutive and non-consecutive) in non-cyclone years (early dry 2016; late wet, early dry and late dry 2018). We were unable to include bushbuck and hartebeest in this analysis owing to low sample sizes in the 2019 wet season. To minimize sample-size imbalance among seasons and species (mean 16.9, minimum 6, maximum 40), we randomly rarefied species' samples from a given season and year to $n = 8$ (when $n > 8$) and calculated average population-level diets and dissimilarity based on this subset. We repeated this process 1,000 times and used the mean value for analysis. We tested whether dissimilarity across the cyclone-affected period was greater than usual using GLMM with beta error distribution, fixed effect of cyclone occurrence, and random intercepts for herbivore species. The inclusion of non-consecutive seasons or years in the baseline for this comparison constitutes a liberal definition of 'normal' seasonal dissimilarity, and a conservative test of cyclone-induced dietary anomaly,

Article

because the baseline includes dissimilarity between disparate seasons or years (for example, dry season 2016 versus wet season 2018).

Herbivore dietary attributes

We quantified diet breadth as the number of plant families per faecal sample (to avoid potentially confounding effects of variation in taxonomic resolution of mOTUs and in sample size per species on richness estimates) in each season (data were available for all seasons in 2018 and 2019, and for the early dry season only in 2016). For each season, we used Poisson GLMMs with fixed categorical effects of year and per-species random intercepts to test if diet breadth was significantly different in the cyclone year, 2019.

To test whether proportional consumption of grasses (RRA of Poaceae mOTUs) shifted in response to cyclone-induced shifts in understory productivity (Fig. 2 and Extended Data Fig. 6a), we used beta GLMMs for each season with fixed categorical effects of year and per-species random intercepts. We modelled mean grass RRA per species rather than per sample to avoid an inordinately large number of zeroes, and we used zero-inflation terms for the dry season models to satisfy model assumptions.

We analysed forage traits using a locally collected plant trait database and published protocols[32]. We focused on six plant traits associated with forage quality and/or hypothesized sensitivity to flooding: mean field-measured height of the plant species (short-statured plants should be more depleted by flooding), foliar digestible protein content (a chief and often limiting macronutrient for herbivores), dry matter digestibility (a key component of diet quality that influences the amount of nutrients animals can extract), lignin (an indigestible component of cell walls that is most abundant in woody plants), phosphorus (a major mineral nutrient), and sodium (a potentially limiting micronutrient). Following ref. 32, we discarded dietary mOTUs that did not match plant taxa in the traits dataset and then recomputed RRA for each sample; we further discarded samples with <60% of original reads remaining after removal of unmatched mOTUs (1,360 of 1,470 samples retained; median reads preserved = 98.1%). We then multiplied the RRA of each mOTU by its trait value to obtain a weighted estimate of each trait in each sample. We tested for differences in these attributes (per sample) using linear mixed-effects models for each season with fixed categorical effects of year and per-species random intercepts; to satisfy model assumptions, plant height was log-transformed, protein was reciprocally transformed, and the other metrics (expressed as proportions) were logit-transformed.

To evaluate interspecific differentiation (dietary niche partitioning), we conducted perMANOVA of dietary dissimilarity between each pair of species in each season and year and used the R^2 statistic as an index of the strength of niche differentiation[33] (higher R^2 values indicate that herbivore species identity explains a larger proportion of variance in dietary dissimilarity). Because perMANOVA is sensitive to sample size, which differed among sampling periods, we randomly rarefied species' samples to $n = 8$, iterated 1,000 times, and used the mean R^2 value in analyses. We analysed R^2 values using beta GLMMs for each season with fixed categorical effects of year and per-species random intercepts.

To test whether herbivore traits mediated cyclone-induced dietary shifts, we focused on three metrics that collectively represent diet composition (between-season turnover), breadth (family-level richness), and quality (digestibility). For breadth and quality, we fit models for each season that included interactive effects of year (cyclone occurrence) and each trait (body mass or habitat affiliation) and report effects of the cyclone×trait interactions; for turnover, the response variable (Z scores of dissimilarity for each species between pre- and post-cyclone seasons and all other season pairs) inherently accounted for cyclone occurrence, so models included only the main effect of each trait. Specific fitting procedures and results are in Extended Data Table 2.

Nutritional condition

Nutritional condition reflects endogenous energy reserves available for maintenance, growth, and reproduction and is a key correlate of fitness in ungulates, influencing survivorship, pregnancy rates, offspring size, and vulnerability to predation[85]. We compared mean nutritional condition of bushbuck ($n = 14$), nyala ($n = 7$), and kudu ($n = 12$) three months after landfall (June–July 2019) with measurements from previous years (June–July 2014, 2015, 2016 and 2018; bushbuck $n = 11, 11, 7$ and 13; nyala $n = 10, 6, 0$ and 4; and kudu $n = 12, 9, 0$ and 18, respectively). Nutritional condition data were collected while animals were immobilized for GPS collaring. We recorded body dimensions (body and hind foot lengths, chest girth), used ultrasound to measure maximum rump-fat depth and thickness of the biceps femoris and longissimus dorsi muscles, and conducted standardized palpation scoring at the sacrosciatic ligament, lumbar vertebrae, sacrum, base of tail, and caudal vertebrae (based on protocols developed for North American ungulates[86]). Because equations for converting these measurements into estimates of ingesta-free body fat have not been validated for African ungulates, we followed an approach that we have previously used for Gorongosa antelopes[34,54,84] to develop an index of relative nutritional condition using principal component analysis (Supplementary Table 3). Metrics associated with body size (for example, muscle thicknesses, body length) loaded most strongly onto PC1, whereas those associated with body fat (for example, palpation scores, maximum fat depth) loaded most strongly onto PC2 (Supplementary Table 4). Thus, we used PC2 as an index of nutritional condition (that is, endogenous fat reserves) and report the inverse of PC2 such that larger values equate to more available fat[34,54,84]. We used Welch's two-sample t-test (Fig. 4e) to test for differences in condition in each species before Idai (2014–2016 and 2018) versus after Idai (2019); note that because we do not recapture collared animals, these analyses reflect mean population-level differences across years rather than individual-level changes through time.

Aerial wildlife surveys

Gorongosa conducts biennial aerial wildlife counts[28]. We used data from 2014, 2016, 2018 and 2020 (in which total counts were conducted within a standardized 193,500-ha block at the core of the park using consistent methodology) to evaluate population trends before versus after Idai. Detailed methods for each count are in refs. 28,87. All counts were conducted in the late dry season (October–November, to enhance visibility) by the same pilot (M. Pingo, Sunrise Aviation) with three experienced observers (always including M.E.S.) in a Bell JetRanger helicopter with all four doors removed. Surveys were conducted at a constant height (50–55 m above the ground) at 96 km h^{-1} along parallel, 500-m wide transects. All animals within 250 m on either side of the centre line were individually counted and their locations recorded using GPS. Large herds were circled for accurate counting; when necessary, photographs were used to enumerate individuals. These total counts should be viewed as minimum estimates of species' true abundance. A carcass count on 14 November 2020 using the same survey methods along a dedicated 250-km transect (6.5% of the count block) revealed 367 dead waterbuck, which was extrapolated to the scale of the count block based on the distribution of carcass density across floodplain and woodland habitats[87].

We used count data from 2014–2018 to quantify study species' habitat affiliation under non-cyclone conditions. Following ref. 54, we quantified the mean proportion of individuals of each species in floodplain grassland habitat (the treeless area around Lake Urema, as delineated by a pre-existing habitat classification[52]) across survey years. We tested whether floodplain affiliation was correlated with body mass using Pearson's product-moment correlation coefficient.

We tested whether proportional changes in abundance before versus after Idai [$(N_{2020} - N_{2018})/N_{2018}$] differed from that observed between consecutive pairs of non-cyclone years (2014–2016, 2016–2018) by

fitting a linear mixed-effects model with Gaussian error distribution, a categorical variable for cyclone incidence as the fixed effect, and per-species random intercepts using glmmTMB. We inspected residuals using simulateResiduals() in DHARMa, yielding no evidence that assumptions were violated. We evaluated whether herbivore species' body mass, habitat affiliation, or diet (mean grass RRA in early dry seasons of 2016 and 2018) predicted population growth/decline before versus after Idai using linear regression. We used AICc for model selection among 16 candidate models, which comprised all combinations of main effects and first-order interactions of the three predictors (Supplementary Table 2).

Reporting summary

Further information on research design is available in the Nature Portfolio Reporting Summary linked to this article.

Data availability

Data used in this study are available on Dryad: https://doi.org/10.5061/dryad.63tj806; https://doi.org/10.5061/dryad.sxksn02zc and https://doi.org/10.5061/dryad.7wm37pvzv. Source data are provided with this paper.

Code availability

Code used in our analyses is available on Dryad: https://doi.org/10.5061/dryad.7wm37pvzv.

51. Guyton, J. A. et al. Trophic rewilding revives biotic resistance to shrub invasion. *Nat. Ecol. Evol.* **4**, 712–724 (2020).
52. Stalmans, M. & Beilfuss, R. *Landscapes of the Gorongosa National Park* (Gorongosa National Park, 2008).
53. Pansu, J. et al. Trophic ecology of large herbivores in a reassembling African ecosystem. *J. Ecol.* **109**, 1355–1376 (2019).
54. Atkins, J. L. et al. Cascading impacts of large-carnivore extirpation in an African ecosystem. *Science* **364**, 173–177 (2019).
55. Bouley, P., Poulos, M., Branco, R. & Carter, N. H. Post-war recovery of the African lion in response to large-scale ecosystem restoration. *Biol. Conserv.* **227**, 233–242 (2018).
56. Bouley, P., Paulo, A., Angela, M., Du Plessis, C. & Marneweck, D. G. The successful reintroduction of African wild dogs (*Lycaon pictus*) to Gorongosa National Park, Mozambique. *PLoS ONE* **16**, e0249860 (2021).
57. Cabral, P. et al. Assessing Mozambique's exposure to coastal climate hazards and erosion. *Int. J. Disaster Risk Reduct.* **23**, 45–52 (2017).
58. Kolstad, K. W. Predictions and precursors of Idai and 38 other tropical cyclones and storms in the Mozambique Channel. *Q. J. R. Meteorol. Soc.* **147**, 45–57 (2021).
59. Nhundu, K., Sibada, M. & Chaminuka, P. in *Cyclones in Southern Africa* (Springer, 2021).
60. Kingdon, J. *The Kingdon Field Guide to African Mammals* (Bloomsbury, 1997).
61. R Core Team, *R: A Language and Environment for Statistical Computing*. http://www.R-project.org/ (R Foundation for Statistical Computing, 2020).
62. Pebesma, E. Multivariable geostatistics in S: the gstat package. *Comput. Geosci.* **30**, 683–691 (2004).
63. UNOSAT. *Cumulative Satellite Detected Waters Extent Overview Between 13 & 26 March 2019 over Sofala province, Mozambique*. https://data.humdata.org/dataset/cumulative-satellite-detected-waters-extent-13-26-march-2019-over-sofala-province-mozambique (UNITAR, 2019).
64. Western, D., Mose, V. N., Worden, J. & Maltumo, D. Predicting extreme droughts in savannah Africa: a comparison of proxy and direct measures in detecting biomass fluctuations, trends, and their causes. *PLoS ONE* **10**, e0136516 (2015).
65. Busetto, L. & Ranghetti, L. MODIStsp: an R package for automatic preprocessing of MODIS Land Products time series. *Comput. Gosci.* **97**, 40–48 (2016).
66. Kilsch, A. & Atzberger, C. Operational drought monitoring in Kenya using MODIS NDVI time series. *Remote Sens.* **8**, 267 (2016).
67. Mamugy, F. *Does Predation or Competition Shape the Home Range and Resources Selection by Sable Antelope (Hippotragus niger) in the Gorongosa National Park, Mozambique?* MSc thesis, University of the Witwatersrand (2016).
68. Arumoogum, N. *Spatiotemporal Niche Dynamics of a Reassembling Herbivore Ensemble in Southern Africa*. PhD thesis, University of the Witwatersrand (2022).
69. Branco, P. S. et al. Determinants of elephant foraging behavior in a coupled human–natural system: is brown the new green? *J. Anim. Ecol.* **88**, 780–792 (2019).
70. Animal Care and Use Committee of the American Society of Mammalogists. 2016 Guidelines of the American Society of Mammalogists for the use of wild animals in research and education. *J. Mammal.* **97**, 633–688 (2016).
71. Avgar, T., Potts, J. R., Lewis, M. A. & Boyce, M. S. Integrated step selection analysis: bridging the gap between resource selection and animal movement. *Methods Ecol. Evol.* **7**, 619–630 (2016).
72. Muff, S., Signer, J. & Fieberg, J. Accounting for individual-specific variation in habitat-selection studies: efficient estimation of mixed-effects models using Bayesian or frequentist computation. *J. Anim. Ecol.* **89**, 80–92 (2019).
73. Tarnita, C. et al. A theoretical foundation for multi-scale regular vegetation patterns. *Nature* **541**, 398–401 (2017).
74. Fortin, D. et al. Wolves influence elk movements: behavior shapes a trophic cascade in Yellowstone National Park. *Ecology* **86**, 1320–1330 (2005).
75. Therneau, T. survival: A package for survival analysis in R. R package version 3.5-5. https://cran.r-project.org/web/packages/survival/index.html (2020).
76. Flemming, C. H. et al. Estimating where and how animals travel: an optimal framework for path reconstruction form autocorrelated tracking data. *Ecology* **97**, 576–582 (2016).
77. Mueller, T., Olson, K. A., Leimgruber, P. & Calabrese, J. M. Rigorous home-range estimation with movement data: a new autocorrelated kernel-density estimator. *Ecology* **96**, 1182–1188 (2015).
78. Singer, J., Fieberg, J. & Avgar, T. Animal movement tools (amt): R package for managing tracking data and conducting habitat selection analyses. *Ecol. Evol.* **9**, 880–890 (2019).
79. Brooks, M. E. et al. glmmTMB balances speed and flexibility among packages for zero-inflated generalized linear mixed modeling. *R. J.* **9**, 378–400 (2017).
80. Hartig, F. DHARMa: Residual diagnostics for hierarchical (multi-level/mixed) regression models. R package version 0.3.2.0. https://cran.r-project.org/web/packages/DHARMa/vignettes/DHARMa.html (2022).
81. Giguet-Covex, C. et al. Long livestock farming history and human landscape shaping revealed by lake sediment DNA. *Nat. Comm.* **5**, 3211 (2014).
82. Boyer, F. et al. OBITOOLS: a UNIX-inspired software package for DNA metabarcoding. *Mol. Ecol. Resour.* **16**, 176–182 (2016).
83. Oksanen, J. et al. vegan: Community ecology package. R package version 2.5-6. https://cran.r-project.org/web/packages/vegan/index.html (2020).
84. Walker, R. H. et al. Mechanisms of individual variation in large herbivore diets: roles of spatial heterogeneity and state-dependent foraging. *Ecology* **104**, e3921 (2023).
85. Parker, K. L., Barboza, P. S. & Gillingham, M. P. Nutrition integrates environmental responses of ungulates. *Funct. Ecol.* **23**, 57–69 (2009).
86. Cook, R. C. et al. Revisions of rump fat and body scoring indices for deer, elk, and moose. *J. Wildl. Manag.* **74**, 880–896 (2010).
87. Stalmans, M. E. & Peel, M. Aerial wildlife count of the Gorongosa National Park, Mozambique, November 2020. *Parque Nacional da Gorongosa* https://gorongosa.org/wp-content/uploads/2023/10/GorongosaAerialWildlifeCount2020.pdf (2020).

Author contributions R.H.W., J.A.B., M.C.H., J.H.D., M.E.S., R.M.P. and R.A.L. conceived and designed the study. R.H.W., J.A.B., M.C.H., J.H.D., K.M.G., M.S.P. and R.M.P. performed statistical analyses. J.H.D. and J.D. provided flood depth data. R.H.W., J.A.B., R.M.P., and R.A.L. provided antelope movement data. D.D.G. and R.A.L. provided elephant movement data. N.A., F.P. and J.P.M. provided sable movement data. A.B.P., M.C.H., and R.M.P. provided diet data. K.M.G. and M.S.P. provided camera-trap data. M.A., A.P. and P.B. provided carnivore data. M.E.S. provided aerial survey data. R.H.W. created all data visualizations. R.M.P. and R.A.L. supervised the research. R.H.W., M.C.H., R.M.P. and R.A.L. wrote the manuscript. All authors provided comments and edits.
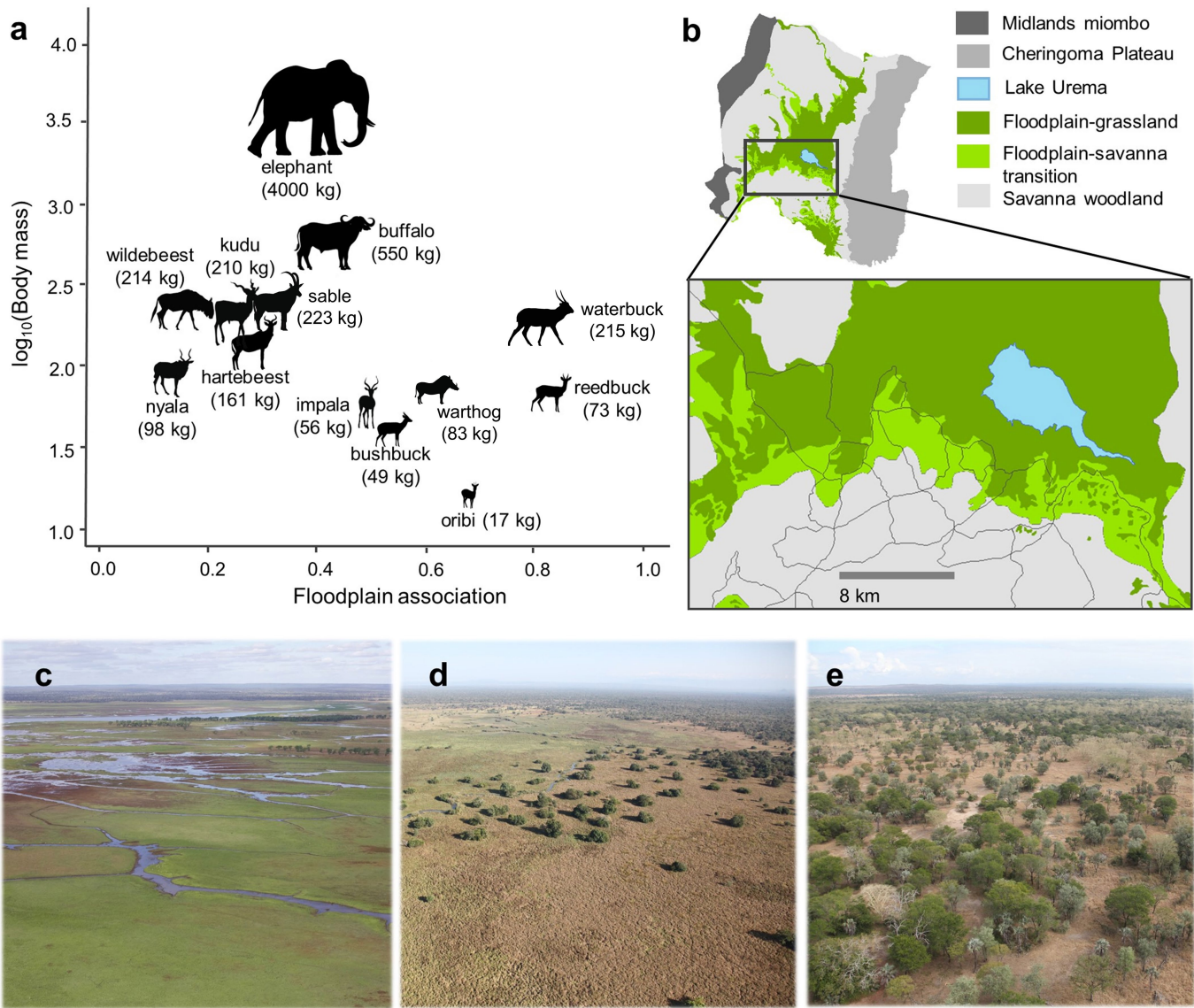
Extended Data Fig. 1 | Herbivore body size and habitat affiliation in Gorongosa. (**a**) The 13 herbivore species in this study spanned a broad spectrum of body sizes and habitat affiliations. Body mass estimates used in this study are the average of sex-specific adult values from ref. 60. Floodplain affiliation is the mean proportion of individuals of each species occurring in floodplain-grassland habitat (**b**,**c**) during aerial wildlife counts (2014–2018). Body mass and floodplain affiliation were uncorrelated ($r = -0.34$, df = 11, $P = 0.26$). (**b**) Map of study area, showing habitat types and geographic features. **c**–**e**, Representative photos of floodplain (**c**, 8–20 m above sea level); floodplain-savanna transition (**d**, 20–25 m above sea level); and savanna woodland (**e**, >25 m above sea level).
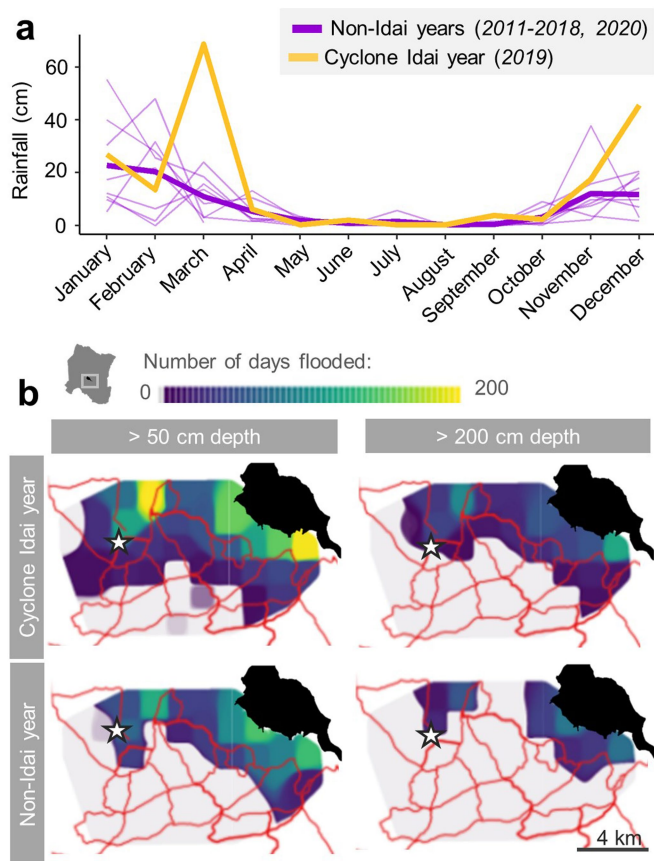
Extended Data Fig. 2 | Rainfall from Cyclone Idai caused extreme and unseasonal flooding. (**a**) Bold yellow line shows monthly rainfall in the year of Cyclone Idai (2019); thin purple lines show monthly rainfall in other years (2011–2018, 2020); bold purple line shows mean monthly rainfall across those years. March of 2019 was roughly fivefold wetter (688 mm) than a typical March (130 mm), and 2019 had roughly twice as much rain (1874 mm) as the long-term annual average (850 mm). (**b**) Floodwaters extended farther (visualized in relation to the road network, red lines) and persisted longer (color scale) in 2019 (top maps) than in 2020 (also a wetter than average year, 1037 mm; bottom maps). Stars mark the location of Lion House, a local landmark. (**c**) Lion House before Idai (early March 2019) when the seasonal flood waters had largely receded in the surrounding floodplain. This photo was taken via drone by the Gorongosa Restoration Project. (**d**) Lion House was submerged by flood waters following Idai, with only the roof remaining above water (photo date: 22 March 2019). This picture was taken from a helicopter during post-Idai humanitarian aid efforts by the Gorongosa Restoration Project. Over two days (15–17 March 2019; **e**-**h**), flooding induced by Cyclone Idai rose by more than 3 m adjacent to Lion House and persisted for 2 months (**i,j**). Photos courtesy of Piotr Naskrecki.
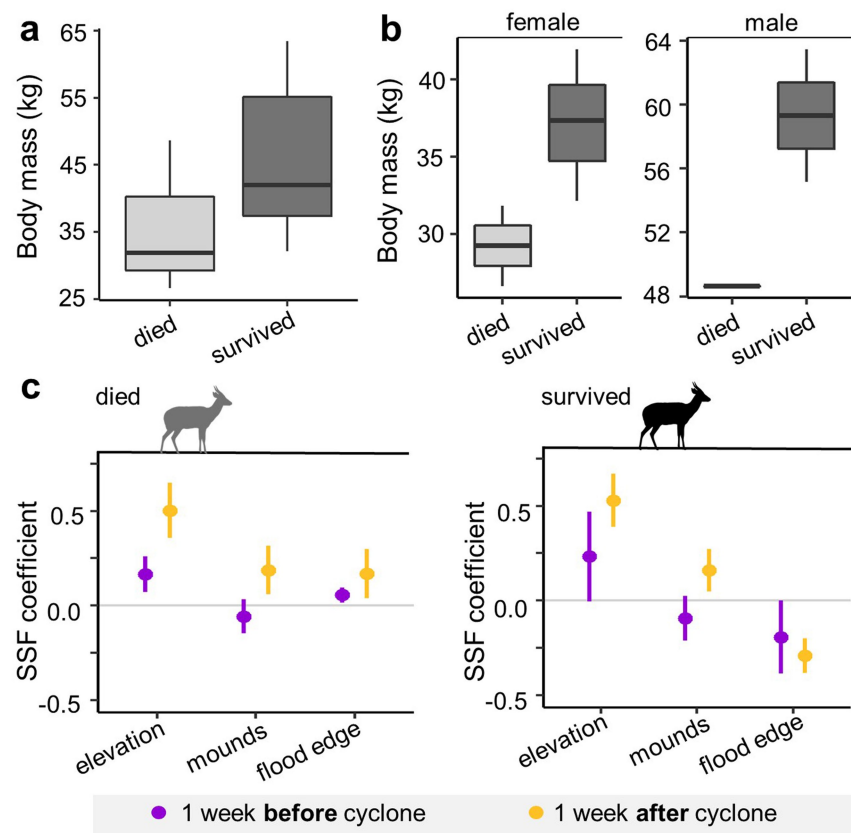
Extended Data Fig. 3 | Body sizes and movement behaviors of bushbuck that died (*n* = 3) and survived (*n* = 5) Cyclone Idai. a–b, The three bushbuck that died in the flood were smaller than the survivors (**a**) and included the two smallest of five adult females and the single smallest of three adult males (**b**). Boxplots show median and interquartile range; whiskers show minimum and maximum. (**c**) Coefficients ± 95% confidence intervals (CIs) from step-selection functions (SSFs) that quantified selection for elevation, termite mounds, and distance to floodwaters in the week before (purple) and after (yellow) Idai.

Positive coefficients indicate selection and negative coefficients indicate avoidance; CIs not overlapping zero indicate significant selection or avoidance; CIs not overlapping each other indicate significant differences before vs. after landfall. Although bushbuck killed by Cyclone Idai significantly increased their selection for higher elevations and mounds (non-overlapping CIs for all coefficients before vs. after landfall), they were unable to avoid the flood edge (indicated by positive coefficients) and died in water >1.5-m deep.
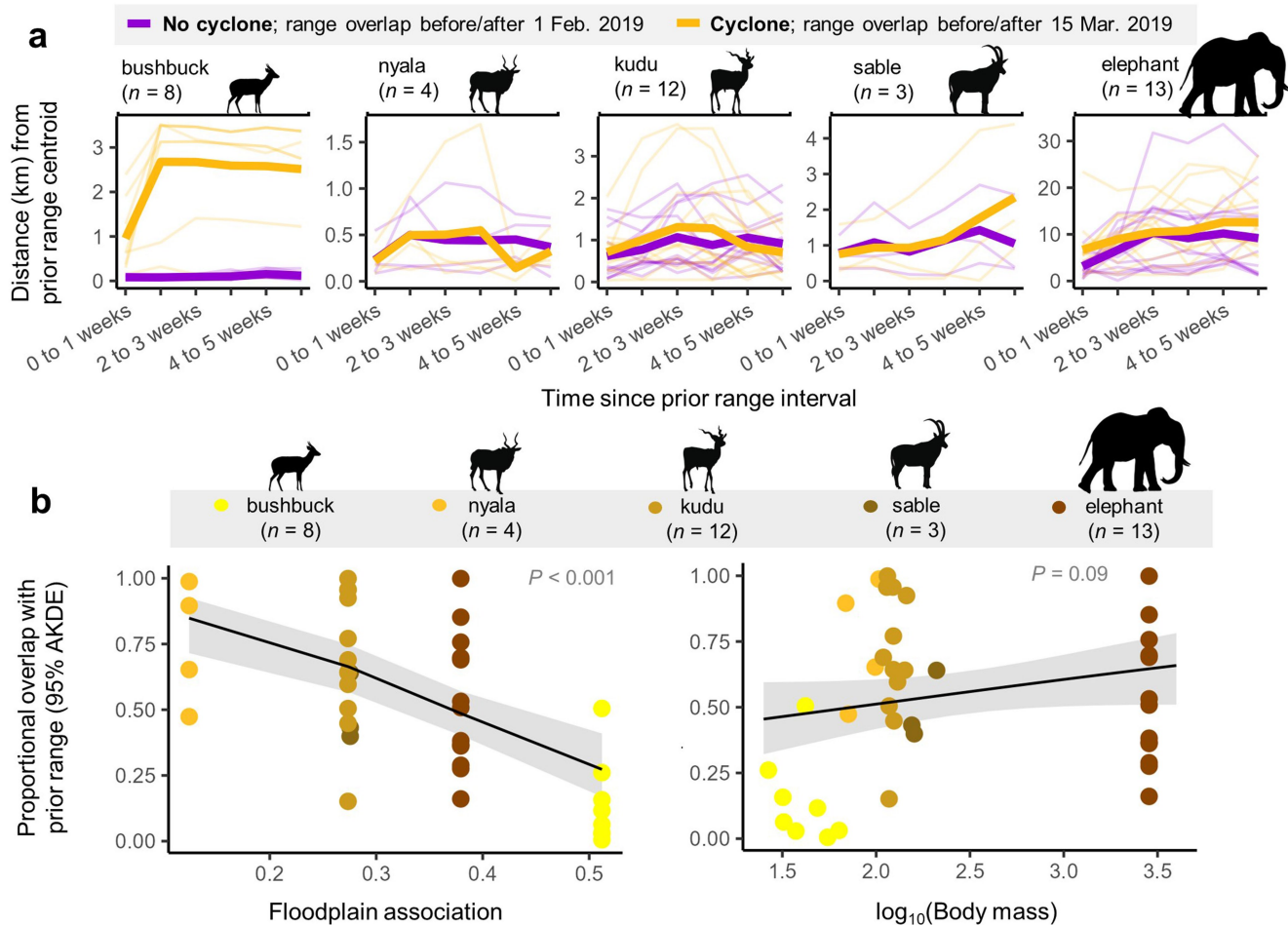
Extended Data Fig. 4 | Herbivore traits predicted degree of displacement after Idai. (**a**) This analysis parallels and complements Fig. 2b, which shows displacement from ranges based on overlap of utilization distributions via 95% autocorrelated kernel density estimation. Thin lines show individual movements; thick lines show the mean across individuals (purple, pre-cyclone; yellow, post-cyclone). Within a week of landfall, bushbuck (2019: $n = 8$) moved many-fold farther from their prior week-long range centroids than expected based on pre-cyclone behavior (Welch's two sample t-test: $\overline{X}_{cyclone} = 0.95$, $\overline{X}_{no\,cyclone} = 0.08$, $t = 3.01$, $P = 0.02$); this effect intensified over the next week ($\overline{X}_{cyclone} = 2.67$, $\overline{X}_{no\,cyclone} = 0.08$, $t = 5.62$, $P < 0.001$) and then persisted over the next month. Some individuals of other herbivore species exhibited similarly anomalous displacement from their prior week-long range centroids after the cyclone (compare thin lines), but these trends were not pronounced at the population level (all $P > 0.05$). (**b**) Affiliation with low-elevation floodplain habitat (quantified at the species level; see Extended Data Fig. 1) strongly predicted the magnitude of individuals' displacement in the week after Idai (i.e., lower overlap with prior home ranges, estimated as utilization distributions via autocorrelated kernel density estimation; mixed-effects model with beta error distribution, fixed effects of floodplain affiliation and log-transformed body mass, and per-species random intercepts: $\beta_{floodplain} = -5.44 \pm 1.65$ s.e., $P = 0.001$). Small size (measured or estimated at the individual level for all species except elephant; see Methods) was also associated with greater displacement after accounting for effects of habitat affiliation ($\beta_{log(mass)} = 0.53 \pm 0.25$ s.e., $P = 0.03$). Model-predicted effects (black line with shaded 95% CI) show strength and direction of each relationship.
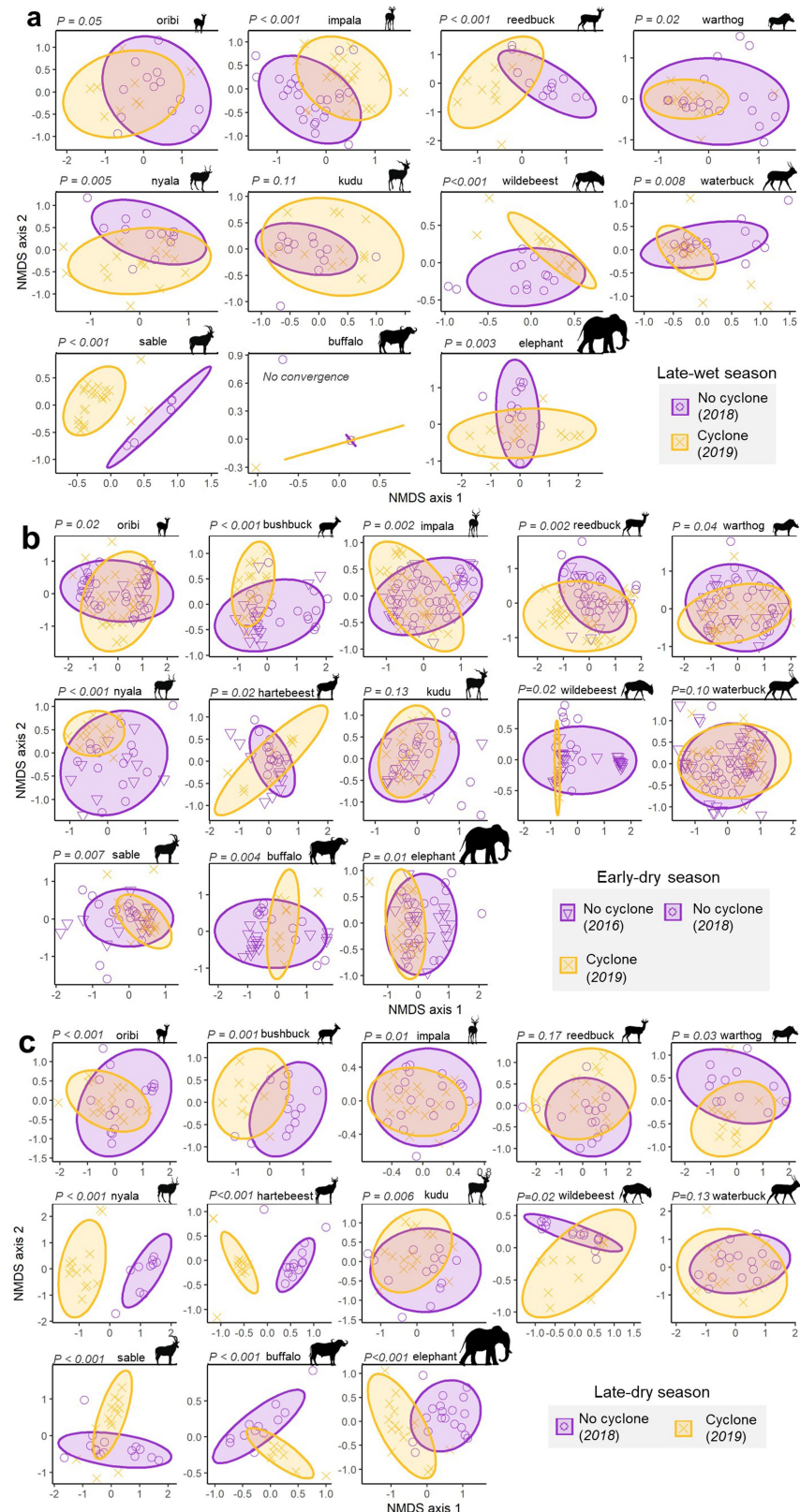
Extended Data Fig. 5 | See next page for caption.

Extended Data Fig. 5 | Herbivore diet composition differed after Cyclone Idai (2019) relative to non-cyclone years (2018, 2016). a–c, Nonmetric multidimensional scaling (NMDS) ordinations of Bray-Curtis dietary dissimilarity based on fecal DNA metabarcoding for each species in each season. Each point corresponds to an individual fecal sample, and distance between points reflects degree of dissimilarity; ellipses show 95% CI derived from the multivariate *t*-distribution and represent diet composition and breadth for each species in the late-wet season (**a**), early-dry season (**b**), and late-dry season (**c**). Sample sizes are in Supplementary Table 1. 2016 data were available only for the early-dry season (**b**), and bushbuck and hartebeest are omitted from the wet season plots (**a**) owing to insufficient sample sizes. *P*-values above each ordination plot are from pairwise permutational analyses of variance (perMANOVA) between cyclone and non-cyclone periods for each species in each season (for the early-dry season, 2016 and 2018 data are plotted separately but lumped as one 'non-cyclone' group for perMANOVA). The perMANOVA for buffalo in the early-dry season failed to converge; all but 5 of the remaining 36 tests indicated statistically significant (*P* ≤ 0.05) dietary differences between cyclone and non-cyclone periods; the only exceptions were kudu in the late-wet and early-dry seasons, waterbuck in the early- and late-dry seasons, and reedbuck in the late-dry season.
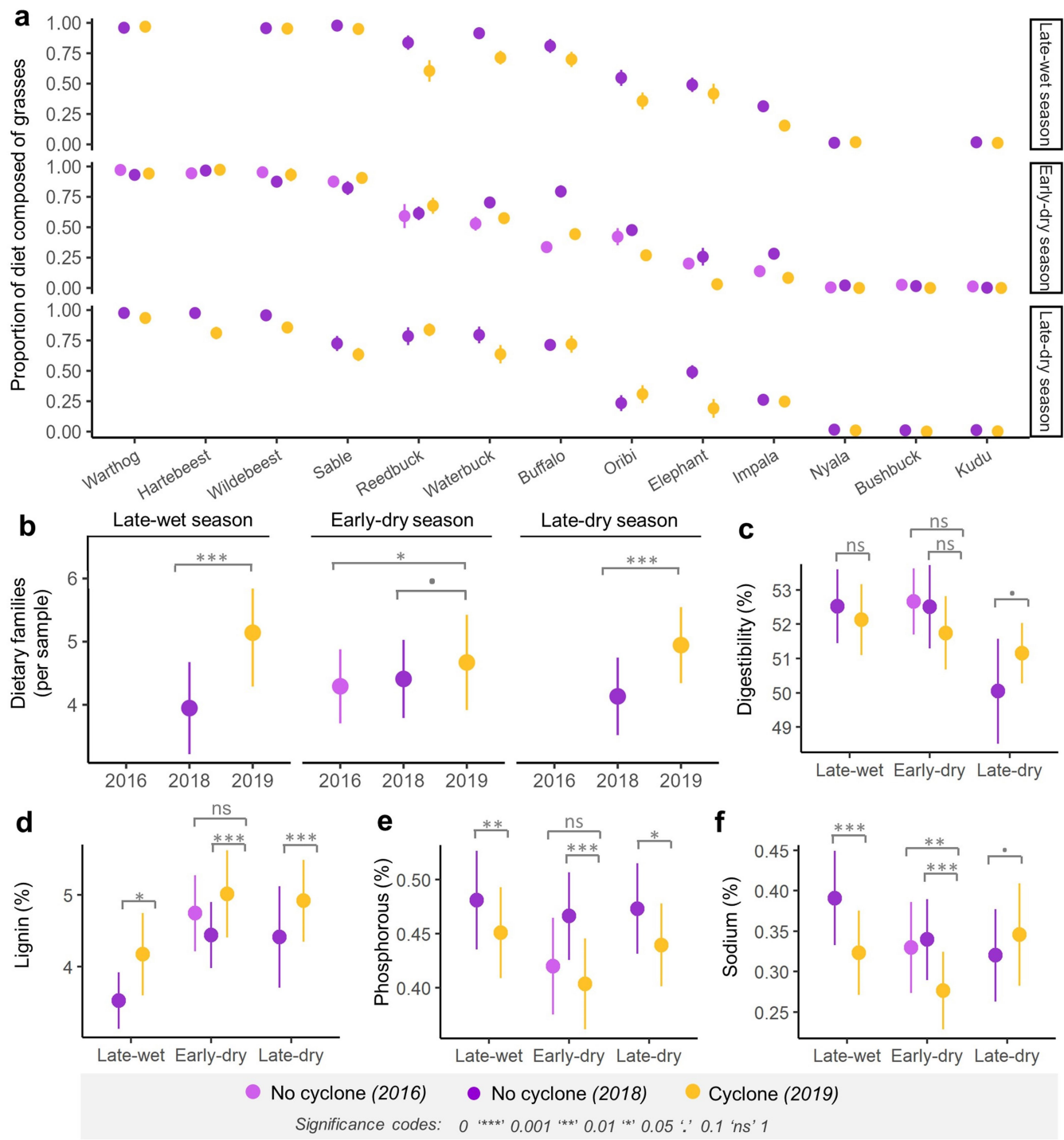
Extended Data Fig. 6 | See next page for caption.

Extended Data Fig. 6 | Herbivore diet metrics after Idai (2019) relative to non-cyclone years (2016, 2018). Points and error bars show mean ± s.e.m; sample sizes are in Supplementary Table 1. Asterisks show statistical significance level, as per legend key at the bottom. (**a**) Relative read abundance (RRA) of grasses in the diet of each species (from left to right in decreasing order of grass consumption). Grass RRA was significantly lower in all seasons after Cyclone Idai than in 2018 (a wetter than average year), but not relative to the 2016 early-dry season (a drier than average year) (beta generalized linear mixed-effects models, with fixed effect of year and per-species random intercepts: wet, $\beta_{2018} = 0.73 \pm 0.12$ s.e., $P < 0.001$; early-dry, $\beta_{2016} = 0.12 \pm 0.21$, $P = 0.56$ and $\beta_{2018} = 0.57 \pm 0.23$, $P = 0.01$; late-dry, $\beta_{2018} = 0.46 \pm 0.19$, $P = 0.02$). (**b**) Family-level dietary richness was greater in all seasons after Idai than in previous years (Poisson mixed-effects model, per-species random intercepts: late-wet, $\beta_{2018} = -0.29 \pm 0.04$ s.e., $P < 0.001$; early-dry, $\beta_{2016} = -0.09 \pm 0.04$, $P = 0.02$ and $\beta_{2018} = -0.06 \pm 0.04$, $P = 0.09$; late-dry, $\beta_{2018} = -0.17 \pm 0.04$, $P < 0.001$). **c**–**e**, We fit separate linear mixed-effects models with per-species random intercepts for measures of diet quality in each season. (**c**) Digestibility was non-significantly lower after Idai in the late-wet ($\beta_{2018} = 0.01 \pm 0.02$, $P = 0.49$) and early-dry seasons ($\beta_{2016} = 0.03 \pm 0.02$ s.e., $P = 0.14$ and $\beta_{2018} = 0.03 \pm 0.02$ s.e., $P = 0.15$); although digestibility was higher on average in the late-dry season ($\beta_{2018} = -0.05$, $SE = 0.02$, $P = 0.05$), this trend conceals strong interactions between the cyclone and herbivore traits, with small-bodied and floodplain-affiliated species having less digestible diets after Idai than in 2018 (see Extended Data Table 2). (**d**) Lignin content was elevated throughout the year after Idai (late-wet, $\beta_{2018} = -0.10 \pm 0.04$, $P = 0.01$; early-dry, $\beta_{2016} = -0.05 \pm 0.03$, $P = 0.15$ and $\beta_{2018} = -0.12 \pm 0.03$, $P < 0.001$; late-dry, $\beta_{2018} = -0.14 \pm 0.04$, $P < 0.001$). (**e**) Phosphorus content was lower after Idai in all seasons (late-wet, $\beta_{2018} = 0.07 \pm 0.03$, $P = 0.005$; early-dry, $\beta_{2016} = 0.04 \pm 0.03$, $P = 0.12$ and $\beta_{2018} = 0.16 \pm 0.03$, $P < 0.001$; late-dry, $\beta_{2018} = 0.07 \pm 0.03$, $P = 0.02$). (**f**) Sodium content was lower after Idai in the late-wet ($\beta_{2018} = 0.25 \pm 0.06$, $P < 0.001$) and early-dry seasons ($\beta_{2016} = 0.21 \pm 0.06$, $P = 0.001$ and $\beta_{2018} = 0.34 \pm 0.06$, $P < 0.001$) but rebounded by the late-dry season ($\beta_{2018} = -0.11 \pm 0.07$, $P = 0.10$).
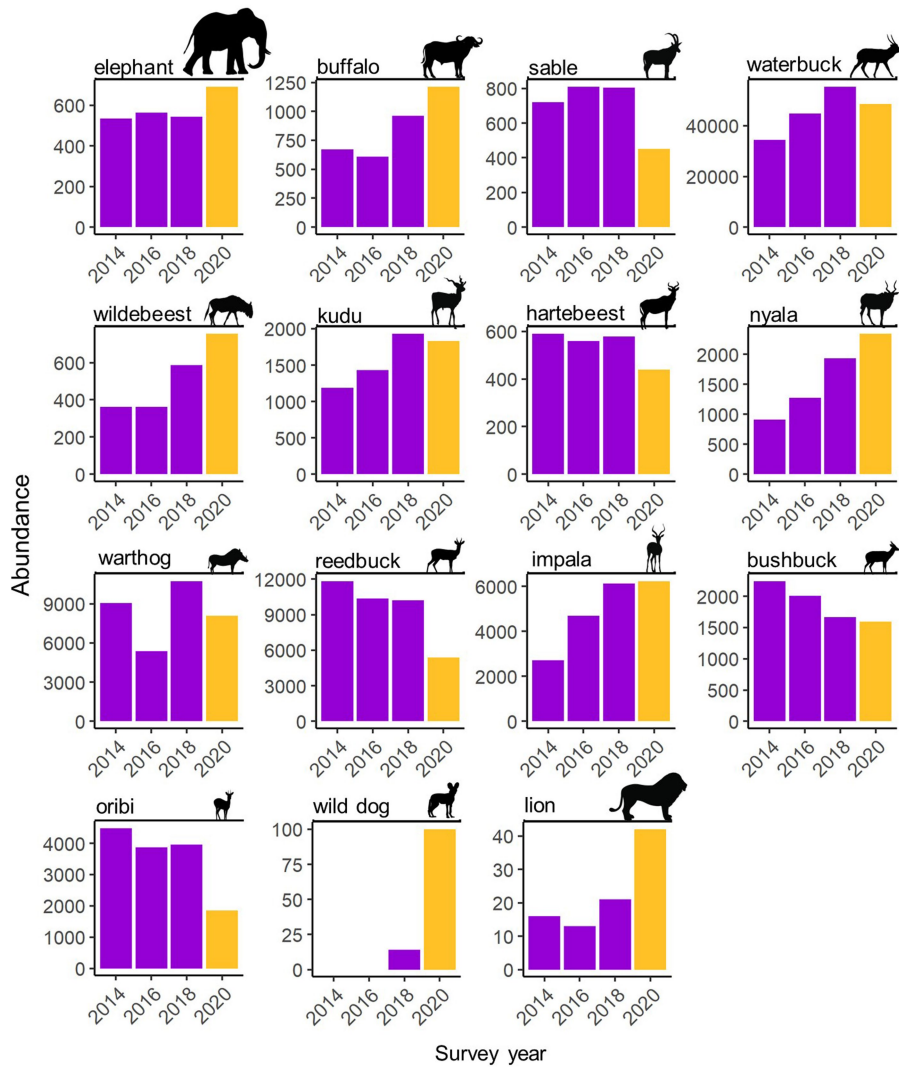
Extended Data Fig. 7 | Large-mammal abundance in the years before and after Idai. Data are from biennial helicopter-based wildlife surveys, except for wild dog for which we used monitoring data from Gorongosa's Conservation Program, and represent systematic total counts covering a standardized 193,500-ha area in the core of the park during the late dry season, when canopy cover is lowest. Even the most meticulous counts do not detect all individuals, so data should be interpreted as minimum numbers known alive, but we are otherwise confident in the accuracy of data for these herbivore populations. Lions are particularly difficult to count from the air, and these data substantially underestimate total abundance inferred from ground-based monitoring[55], but we consider them a qualitatively reliable index of relative abundance across years.
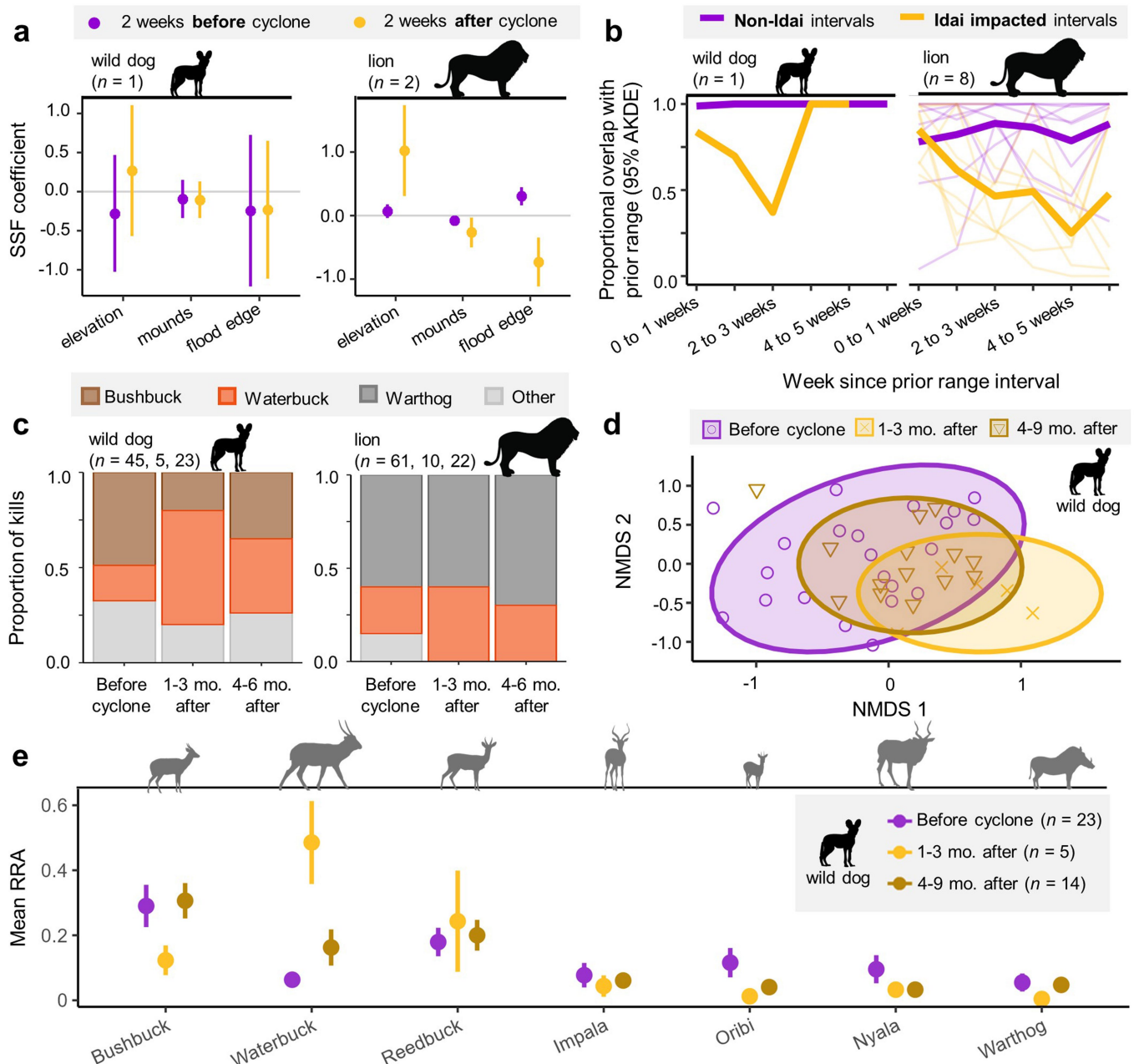
Extended Data Fig. 8 | Carnivore behavior before and after Cyclone Idai.
(**a**) Coefficients ± 95% CIs from step-selection functions (SSFs) fit to GPS
telemetry data from African wild dog (the only pack present at the time of this
study) and lion, showing selection for elevation, termite mounds, and distance
to flood waters in the two weeks before (purple) and after (yellow) Idai (cf. Fig. 2a).
(**b**) Both species exhibited moderate displacement from their ranges, moving
away from Lake Urema in the weeks after landfall (yellow lines compare the
week prior to 15 Mar. 2019 to weekly bins thereafter; thin, individuals; bold,
population) relative to periods immediately before the cyclone (purple lines
compare the week prior to 1 Feb. 2019 to weekly bins thereafter; cf. Fig. 2b).

c–**e**, Whereas no shift in lion diet was detected, the proportion of waterbuck
among confirmed wild dog kills increased after the cyclone (**c**; sample sizes
for each time period at top). This shift was associated with a greater overall
difference in wild dog diet composition before versus immediately after the
cyclone as quantified using DNA metabarcoding and visualized here by
nonmetric multidimensional scaling (NMDS) ordination of Bray Curtis
dissimilarity values (**d**; markers correspond to individual fecal samples).
Relative read abundance (RRA) of prey DNA in wild dog scats independently
the general pattern observed in the kill data (**e**; means ± s.e.m.).

Article

Extended Data Table 1 | Parameter estimates from species-specific models of monthly herbivore distribution (proportion of detections at each camera location) after March 15ᵗʰ in the cyclone year (2019) versus two non-cyclone years (2017, 2018)

Waterbuck (*Kobus ellipsiprymnus*)	*β*	s.e.	*P*-value
Intercept	**11.83**	**2.86**	**< 0.001**
cyclone	**-17.40**	**4.46**	**< 0.001**
lake	**-2.06**	**0.32**	**< 0.001**
month	-0.70	0.50	0.16
cyclone:lake	**1.99**	**0.50**	**< 0.001**
cyclone:month	**2.33**	**0.86**	**0.007**
lake:month	0.07	0.06	0.22
cyclone:lake:month	**-0.26**	**0.10**	**0.006**

Warthog (*Phacochoerus africanus*)	*β*	s.e.	*P*-value
Intercept	**10.67**	**2.80**	**< 0.001**
cyclone	**-22.68**	**4.08**	**< 0.001**
lake	**-1.97**	**0.31**	**< 0.001**
month	**-1.46**	**0.39**	**< 0.001**
cyclone:lake	**2.53**	**0.45**	**< 0.001**
cyclone:month	**3.83**	**0.83**	**< 0.001**
lake:month	**0.17**	**0.04**	**< 0.001**
cyclone:lake:month	**-0.42**	**0.09**	**< 0.001**

Nyala (*Tragelaphus angasii*)	*β*	s.e.	*P*-value
Intercept	**-19.40**	**6.21**	**0.002**
cyclone	-9.86	6.89	0.15
lake	**1.35**	**0.68**	**0.05**
month	-0.04	0.96	0.96
cyclone:lake	1.02	0.75	0.17
cyclone:month	**4.04**	**1.42**	**0.004**
lake:month	0.002	0.11	0.97
cyclone:lake:month	**-0.43**	**0.16**	**0.005**

Impala (*Aepyceros melampus*)	*β*	s.e.	*P*-value
Intercept	**12.66**	**4.60**	**0.006**
cyclone	**-15.22**	**5.23**	**0.004**
lake	**-2.27**	**0.51**	**< 0.001**
month	**-2.76**	**0.55**	**< 0.001**
cyclone:lake	**1.77**	**0.57**	**0.002**
cyclone:month	**2.85**	**1.05**	**0.007**
lake:month	**0.32**	**0.06**	**< 0.001**
cyclone:lake:month	**-0.32**	**0.12**	**0.005**

Bushbuck (*Tragelaphus sylvaticus*)	*β*	s.e.	*P*-value
Intercept	3.70	2.92	0.20
cyclone	-2.11	4.27	0.62
lake	**-1.14**	**0.32**	**< 0.001**
month	-0.22	0.45	0.46
cyclone:lake	0.21	0.47	0.66
cyclone:month	0.45	0.88	0.61
lake:month	0.03	0.05	0.55
cyclone:lake:month	-0.04	0.10	0.67

Columns are generalized linear mixed model parameter estimates (*β*), standard errors (s.e.) and *P*-values. Predictors are distance (m) from Lake Urema ('lake', a continuous variable), log-transformed to adhere to model assumptions; months since 15 March, the date of cyclone landfall in 2019 ('month', continuous); and whether or not a cyclone occurred in the year ('cyclone', binary, '1' for the cyclone year, 0 for non-cyclone years). Boldface denotes statistically significant effects (*P* ≤ 0.05). Coefficients were directionally consistent across species in all but one case and indicate fewer detections after the cyclone, especially near the lake, and especially in the immediate aftermath (Fig. 2c). Our inferences are based primarily on the three-way cyclone:lake:month interaction, with significant effects for 4 of 5 species showing that Idai changed herbivore distributions relative to Lake Urema, and that this effect depended on time since landfall.

Extended Data Table 2 | Summary of cyclone-trait interactions for dietary metrics

Response	Season	Cyclone × Body mass	Cyclone × Habitat affiliation	Summary of cyclone impact
Dietary dissimilarity between seasons (turnover)	N/A	β = -0.22 ± 0.12 P = 0.08	β = 2.18 ± 0.52 P < 0.001	*Turnover before vs. after cyclone (relative to normal inter-season variation) was higher in floodplain-affiliated and small-bodied species*
Family-level dietary richness	Late wet	β = 0.02 ± 0.03 P = 0.49	β = -0.64 ± 0.18 P < 0.001	*Cyclone-associated increase in dietary richness relative to 2018 was greater in floodplain species*
Family-level dietary richness	Early dry	β = 0.01 ± 0.03 P = 0.62 (2016) β = 0.01 ± 0.03 P = 0.70 (2018)	β = -0.17 ± 0.18 P = 0.34 (2016) β = -0.37 ± 0.17 P = 0.03 (2018)	*Cyclone-associated increase in dietary richness relative to 2018 was greater in floodplain species; this trend was not significant for the comparison with 2016*
Family-level dietary richness	Late dry	β = 0.07 ± 0.03 P = 0.007	β = -0.29 ± 0.2 P = 0.15	*Cyclone-associated increase in dietary richness relative to 2018 was greater in small-bodied species*
Dietary digestibility	Late wet	β = -0.02 ± 0.01 P = 0.26	β = -0.13 ± 0.08 P = 0.10	*N/A*
Dietary digestibility	Early dry	β = 0.002 ± 0.02 P = 0.89 (2016) β = -0.01 ± 0.01 P = 0.55 (2018)	β = -0.07 ± 0.09 P = 0.44 (2016) β = -0.03 ± 0.09 P = 0.74 (2018)	*N/A*
Dietary digestibility	Late dry (Oct.–Nov.)	β = -0.10 ± 0.02 P < 0.001	β = 0.39 ± 0.10 P < 0.001	*Cyclone flattened the usual negative scaling of digestibility with size and positive scaling of digestibility with floodplain affiliation, resulting in lower diet quality among small and floodplain species relative to 2018 (cf. Extended Data Fig. 6c)*

For dietary dissimilarity (turnover, top row), we report results (coefficient ± s.e., *P*-value) of linear models containing the focal trait (body mass and habitat affiliation) as the only predictor; the response variable was each species' *Z*-score of dietary dissimilarity between the periods immediately preceding (November 2018) and following (April 2019) Cyclone Idai compared with all other pairs of seasons (as in Fig. 4a). For the other two metrics (family-level dietary richness, dietary digestibility), we report cyclone×trait interactions from generalized linear mixed models containing fixed effects of year, each focal trait, and their interaction, with per-species random intercepts. Models of dietary richness used a Poisson error distribution, models for digestibility (logit-transformed) used a Gaussian distribution. Models for the early-dry season contained interaction terms for each of the non-cyclone years (2016 and 2018).

nature portfolio

Corresponding author(s): R.H. Walker, R.M. Pringle, & R.A. Long

Last updated by author(s): Apr 26, 2023

Reporting Summary

Nature Portfolio wishes to improve the reproducibility of the work that we publish. This form provides structure for consistency and transparency in reporting. For further information on Nature Portfolio policies, see our Editorial Policies and the Editorial Policy Checklist.

Statistics

For all statistical analyses, confirm that the following items are present in the figure legend, table legend, main text, or Methods section.

n/a	Confirmed	
☐	☒	The exact sample size (*n*) for each experimental group/condition, given as a discrete number and unit of measurement
☐	☒	A statement on whether measurements were taken from distinct samples or whether the same sample was measured repeatedly
☐	☒	The statistical test(s) used AND whether they are one- or two-sided *Only common tests should be described solely by name; describe more complex techniques in the Methods section.*
☐	☒	A description of all covariates tested
☐	☒	A description of any assumptions or corrections, such as tests of normality and adjustment for multiple comparisons
☐	☒	A full description of the statistical parameters including central tendency (e.g. means) or other basic estimates (e.g. regression coefficient) AND variation (e.g. standard deviation) or associated estimates of uncertainty (e.g. confidence intervals)
☐	☒	For null hypothesis testing, the test statistic (e.g. *F*, *t*, *r*) with confidence intervals, effect sizes, degrees of freedom and *P* value noted *Give P values as exact values whenever suitable.*
☒	☐	For Bayesian analysis, information on the choice of priors and Markov chain Monte Carlo settings
☐	☒	For hierarchical and complex designs, identification of the appropriate level for tests and full reporting of outcomes
☐	☒	Estimates of effect sizes (e.g. Cohen's *d*, Pearson's *r*), indicating how they were calculated

Our web collection on statistics for biologists contains articles on many of the points above.

Software and code

Policy information about availability of computer code

Data collection	Sequences were curated and filtered using the OBITools bioinformatic pipeline (Boyer et al. 2016).
Data analysis	All statistical analyses were conducted in program R statistical software (version 4.2.2) . We created custom code and previously developed packages for our analyses, including gstat (Pesmada 2004), alphahull (Pateir-Lopex & Rodriquez-Casal 2022), MODIStsp (Busetto and Ranghetti 2016), survival (Therneau 2020), amt (Singer et al. 2019), glmmTMB (Brooks et al. 2017), DHARMa (Hartig 2022), vegan (Oksanen et al. 2020).

For manuscripts utilizing custom algorithms or software that are central to the research but not yet described in published literature, software must be made available to editors and reviewers. We strongly encourage code deposition in a community repository (e.g. GitHub). See the Nature Portfolio guidelines for submitting code & software for further information.

Data

Policy information about availability of data

All manuscripts must include a data availability statement. This statement should provide the following information, where applicable:
- Accession codes, unique identifiers, or web links for publicly available datasets
- A description of any restrictions on data availability
- For clinical datasets or third party data, please ensure that the statement adheres to our policy

All data, code, and materials used in our analysis will be made publicly available upon the acceptance of this manuscript for publication.

Research involving human participants, their data, or biological material

Policy information about studies with [human participants or human data](#). See also policy information about [sex, gender (identity/presentation), and sexual orientation](#) and [race, ethnicity and racism](#).

Reporting on sex and gender	Our research does not include human participants.
Reporting on race, ethnicity, or other socially relevant groupings	Our research does not include human participants.
Population characteristics	Our research does not include human participants.
Recruitment	Our research does not include human participants.
Ethics oversight	Our research does not include human participants.

Note that full information on the approval of the study protocol must also be provided in the manuscript.

Field-specific reporting

Please select the one below that is the best fit for your research. If you are not sure, read the appropriate sections before making your selection.

☐ Life sciences   ☐ Behavioural & social sciences   ☒ Ecological, evolutionary & environmental sciences

For a reference copy of the document with all sections, see [nature.com/documents/nr-reporting-summary-flat.pdf](#)

Ecological, evolutionary & environmental sciences study design

All studies must disclose on these points even when the disclosure is negative.

Study description	We integrated data from multiple, concurrent research projects in Gorongosa National Park, Mozambique to capture individual and population-level responses of large mammals to Cyclone Idai.
Research sample	Our research sample represented the movement, distribution, diet, nutritional condition, and abundance of Gorongosa's two extant large carnivores (lion, Panthera leo, and wild dog, Lycaon pictus) and the 13 most abundant (n > 500 in 2018) and widespread large-herbivore species to Cyclone Idai: savanna elephant (Loxodonta africana), buffalo (Syncerus caffer), sable antelope (Hippotragus niger), wildebeest (Connochaetes taurinus), waterbuck (Kobus ellipsiprymnus), greater kudu (Tragelaphus strepsiceros), hartebeest (Alcelaphus buselaphus), nyala (Tragelaphus angasii), warthog (Phacochoerus africanus), reedbuck (Redunca arundinum), impala (Aepyceros melampus), bushbuck (Tragelaphus sylvaticus), and oribi (Ourebia ourebi). Data were not available for all study species in every analysis. Movement data were available for African wild dog (n = 1), lion (n = 8), elephant (n = 13), sable(n = 3), kudu (n = 12), nyala (n = 4), and bushbuck (n = 8) that were equipped with GPS collars when Idai made landfall; camera traps (n = 30) produced sufficient sample sizes (n > 10 detections per month 2017-2019) only for waterbuck, warthog, nyala, impala, and bushbuck; and nutritional condition data were only available for bushbuck (n = 56), nyala (n = 27), and kudu (n = 51). Diet and abundance data were available for all study species.
Sampling strategy	We tracked flood depths throughout the main road network in Gorongosa before and after Cyclone Idai using loggers deployed in 2018. Of the 46 flood loggers deployed, 34 had intact data that were included in our analyses. We additionally used publicly available geospatial data on flooding in Mozambique after Cyclone Idai from the UN Operational Satellite Applications Programme (UNOSAT), which includes satellite-detected surface waters (10-m resolution) in the central provinces of Mozambique, as observed from Sentinel-1 imagery acquired from 13–26 March 2019. We calculated NDVI from MODIS data downloaded using the MODIStsp package in R. Movement data from GPS-collared bushbuck (n = 8), nyala (n = 4), kudu (n = 12), sable (n = 3), elephant (n = 13), wild dog (n = 1 pack), and lion (n = 8) were collected as part of ongoing, long-term studies in Gorongosa. A single pack of 14 African wild dogs was reintroduced in June 2018, and the dominant female of that pack had an active GPS collar during our study; because African wild dogs are an obligately social species that live and hunt communally and there were no other packs in the park during our study, we considered the movement data from this female to be representative of the entire wild dog population in Gorongosa. Data on mammals' spatial distribution were from a systematic long-term camera trap grid established in 2016. Of the 48 cameras deployed at the time of the cyclone, 30 survived the flooding. We limited our analyses to data from the 30 surviving cameras across years (2017-2019) to avoid biasing our results by unbalanced sampling among cameras/years. We additionally thinned camera data to minimize repeated sightings of the same individuals (>15 minutes apart). We summed the remaining detections into month-long bins from 15 March to 15 October in each year. Five herbivore species—waterbuck, warthog, nyala, impala, and bushbuck—had sufficient data for inclusion in statistical analyses (i.e., >10 sightings in each monthly bin after March 15th in 2017, 2018, and 2019). Data for carnivore diets were generated as part of (1) previously published observations of lion (n = 93) and wild dog (n = 71) kills in Gorongosa from 2017–2020, and (2) DNA metabarcoding of wild dog scats. To avoid pseudoreplication, we combined scat samples collected on the same date because wild dogs hunt, kill, and eat together, and more than one scat was often collected from the same

den/kill on the same day. We therefore averaged the composition of these samples, yielding a final sample count of n = 42 for metabarcoding analyses.

Data on herbivore diets were generated as part of a long-term study of the Gorongosa food web. The final dataset comprised 13 herbivore species, 1470 fecal samples, and 332 mOTUs. To minimize sample-size imbalance among seasons and species (mean = 16.9, min = 6, max = 40) in our evaluation of dietary turnover, we randomly rarefied a species' samples from a given collection period (season and year) to n = 8 (when n > 8) and calculated average population-level diets and dissimilarity based on this subset. We followed a similar approach in our evaluation of dietary differentiation using the R2 value from pairwise perMANOVAs among each pair of species in each season/year. Because the results of perMANOVAs can be influenced by sample size and sample sizes differed among sampling periods, we randomly rarefied species' samples to reduce inter-annual differences between sample sizes. Species represented by n > 8 samples in a sampling period were randomly rarefied to n = 8 samples, this procedure was repeated 1000 times, and the mean R2 value across iterations was used in analyses.

Data on nutritional condition were collected during capture and collaring as part of an ongoing study of spiral-horned antelopes in Gorongosa. We compared mean nutritional condition of randomly sampled bushbuck (n = 14), nyala (n = 7), and kudu (n = 12) after Cyclone Idai's landfall (June–July 2019) with mean condition of these species in years prior to the cyclone (June–July 2014, 2015, 2016, and 2018; yearly sample sizes, respectively: bushbuck: n = 11, 11, 7, 13; nyala: n = 10, 6, 0, 4; kudu: n = 12, 9, 0, 18).

Data from aerial wildlife counts were collected as part of Gorongosa's monitoring program.

Data collection

JHD and JD provided flood depth data. Flood sensors were deployed inside slotted PVC pipes set vertically into the ground and capped with PVC to reduce disturbance by wildlife; pipes were lashed with stainless steel zip ties to rebar stakes driven 60–100 cm into the ground. We measured the depth from ground level to the bottom of each hole in which a sensor was deployed for later corrections of measured water depths above ground.

RHW, JAB, RMP and RAL provided antelope movement data, collected as part of previous and ongoing studies (Atkins et al. 2019, Daskin et al. 2022, Walker et al. 2023). DDG and RAL provided elephant movement data, collected as part of previous and ongoing studies (Branco et al. 2019, Campbell-Staton et al. 2021) NA, FP, and JM provided sable movement data, collected as part of previous studies (Mamugy 2016, Arumoogum 2022). MA, AP, and PB provided predator movement and kill site data, previously published as part of a prior study (Bouley et al. 2022). All animal handling procedures were in accordance with guidelines established by the American Society of Mammalogists and were arpproved by relevant ethical and permitting agencies (see: Ethics oversight).

KMG and MSP provided camera trap data. Cameras were mounted on a suitable tree at a height of 1 m, angled slightly downward and facing towards open areas or small game trails to maximize animal detections and minimize false triggers. Each camera was within 2 km of a road, but no cameras were placed directly alongside or facing roads.

RHW, JAB, RMP, and RAL provided antelope nutritional condition data, which were collected during capture and collaring as part of an ongoing study of spiral-horned antelopes in Gorongosa. While antelope were immobilized, we measured body dimensions (body and hind-foot length, chest girth), collected ultrasonography data (maximum rump-fat depth, thickness of biceps femoris and longissimus dorsi muscles), and conducted standardized palpation scoring of the sacrosciatic ligament, lumbar vertebrae, sacrum, base of the tail, and caudal vertebrae [based on protocols developed for North American ungulates].

ABP, MCH and RMP provided herbivore diet data and carnivore DNA metabarcoding data, which were collected as part of a long-term study of the Gorongosa food web. Fecal samples were collected by driving Gorongosa's road network and opportunistically collecting samples from defecating ungulates. Occasionally, samples were collected from animals immobilized for GPS-collaring. For each sample, we recorded the GPS coordinates of the defecation site and a classification of the surrounding habitat type. We collected samples with unused nitrile gloves and deposited them in labeled, unused zip-lock bags, which we immediately placed on ice in a cooler until we returned to Gorongosa's field laboratory for processing later the same day. There, we homogenized samples within the collection bag, transferred pea-sized subsamples into labeled tubes containing silica bashing beads and DNA conservation and lysis buffer (Xpedition Lysis/Stabilization Solution; Zymo Research, CA), vortexed the tubes for 30 seconds to break up the sample and expose the DNA to the buffer, and stored them at -20°C pending transport to Princeton University for sequencing.

MES provided aerial survey data. Counts were conducted by an experienced pilot with three concurrent observers from a Bell JetRanger helicopter with all four doors removed to enhance visibility. Surveys were conducted at a constant height of 50-55 m above the ground at 96 km hr-1 along a series of parallel, 500-m wide transects. All animals within 250 m on either side of the center line were individually counted and their location recorded using a GPS; when a large herd was observed, the pilot circled to enable an accurate count, and when necessary, photographs were used to count all individuals. MES participated in all aerial surveys, and all surveys were flown by the same pilot (M. Pingo, Sunrise Aviation).

Timing and spatial scale

We tracked flood depths throughout the main road network in Gorongosa before and after Cyclone Idai using loggers deployed in 2018. Between 18 August and 16 November 2018, we installed 46 automated water-level loggers (HOBO U20L-01; Onset Corp., Bourne, MA, USA) in a regular grid with 1.8-km spacing between locations, covering a 120-km2 minimum convex polygon. An additional logger was deployed indoors in the park's research headquarters to record atmospheric pressure, which we later used to correct raw pressure readings from the other sensors (i.e., to obtain pressure of water, independent of air pressure). All sensors were set to record water levels every 4 h. Between June and September 2019, as floodwaters receded and deployment sites became accessible, we retrieved logger data.

We restricted spatial extent of NDVI analyses to within the remotely sensed area of Idai-induced flooding within the Gorongosa Rift Valley and a 748-km2 polygon defined by the movements of GPS-collared antelopes in 2014–2019 that encompassed the floodplain margin and adjacent higher-elevation savanna-woodland habitats. To evaluate how the increased extent and duration of flooding after Cyclone Idai impacted vegetation productivity, and hence the availability of green forage for herbivores, we compared the mean monthly normalized difference vegetation index (NDVI) curves from 2019 with those from 20 bracketing years (2000-2018, 2020).

Cameras (Bushnell TrophyCamTM) were deployed over a 300-km2 area south of Lake Urema in the center of 5-km2 hexagonal cells, such that each camera was ~2.4 km from six nearest neighbors. We summed detections in to monthly bins after March 15th in 2017,

2018, and 2019.

We partitioned carnivore diet data into three periods—before cyclone, 1–3 mo. after landfall, and 4–9 mo. after landfall—to explore how prey selection changed after Cyclone Idai.

Herbivore diet samples were collected within Gorongosa's road network before (2016, 2018) and after (2019) the cyclone in three seasons: the late wet season (April–May), early dry season (June–July, 2016 only), and late dry season (October–November).

We sampled antelope nutritional condition in three months after Cyclone Idai's landfall (June–July 2019), when flood waters had receded to an extent comparable to the days before Idai's landfall but forage had not yet recovered in the flood zone, and in the same period in years prior to the cyclone (June–July 2014, 2015, 2016, and 2018).

Aerial surveys were conducted in 2014, 2016, 2018, and 2020 (the four years in which a total count was conducted within a standardized 193,500-ha block at the core of the park) to evaluate population trends before versus after Idai.

Data exclusions

We truncated flood sensor data from 16 November 2018 at 04:00 to 21 June 2019 at 08:00.

In our NDVI analyses, we retained only pixels with quality labels 0 or 1 (indicating unobscured pixels), usefulness labels <3 (highest quality estimates), and land labels of 1 (indicating pixel values did not represent water); other pixels were assigned 'NA'.

We rarified GPS data to include only individuals in separate herds or prides to ensure movement behaviors were independently sampled. We limited all observed and random steps to the extent of the LiDAR-derived products from which we extracted environmental covariates; one kudu was thus excluded from SSF analysis because its home range did not overlap with the extent of environmental covariates. Only two of eight GPS collars on lions in the weeks before and after Idai collected data at regular intervals and were appropriate for SSF analysis.

For carnivore diet analyses, one outlier sample (for which 96% of RRA came from the African civet, Civetticis civetta) was excluded from this analysis because this sample may have been civet feces misidentified as a wild-dog scat.

In our evaluation of herbivore dietary turnover, we excluded bushbuck and hartebeest owing to low sample sizes in the 2019 late-wet season.

Reproducibility

Not relevant with our study design.

Randomization

Not relevant with our study design.

Blinding

Not relevant with our study design.

Did the study involve field work?   ☒ Yes   ☐ No

Field work, collection and transport

Field conditions

Gorongosa National Park is located at the southern end of the Great Rift Valley (18.96°, 34.36°) approximately 100 km from the Mozambique Channel. The Rift Valley runs through the center of the Gorongosa National Park and encompasses Lake Urema, a large (dry season extent: 18 km2), shallow (dry season depth: 1.5 m) body of water fed by multiple rivers within the 9300-km2 Urema catchment. Most annual rainfall (mean: 850 mm, IQR 650–1080 mm between 1957 and 2018) occurs during a single wet season from November–April; in that period, Lake Urema expands and floods a large portion of the Rift Valley floor (up to 780 km2) 36,37. When floodwaters recede as the dry season progresses (May–October), water becomes increasingly scarce and Lake Urema persists as a critical perennial water source.

Location

Our study area encompassed the region south and west of Lake Urema, an area that is largely accessible by dirt roads and supports dense concentrations of wildlife. Within this area, vegetation structure and hydrology distinguish three habitat types: (1) floodplain-grassland (8–20 m above sea level), a seasonally flooded, highly productive lawn of grasses and forbs that supports a large portion of Gorongosa's ungulate biomass, (2) floodplain-savanna transition (20–25 m above sea level), characterized by intermittent, short-duration flooding and stands of water-tolerant trees (e.g., fever trees, Vachellia xanthophoea; white acacia, Faidherbia albida; and palms, Hyphaene spp.), and (3) savanna woodland (> 25 m above sea level), an infrequently flooded region with a diverse community of tree species and a full continuum of canopy cover.

Access & import/export

Field work was conducted with permission from the Republic of Mozambique and Gorongosa National Park. Before import into the United States, each herbivore diet sample was subjected to an antiviral treatment (72°C for 30 minutes) as mandated by US Department of Agriculture AHPIS permits to RMP (122489, 123156, 130123).

Disturbance

Flood sensors, camera traps, diet sampling, and aerial wild life surveys induced minimal disturbance in our study system. All animal capture and collaring was conducted in accordance with guidelines established by the American Society of Mammalogists to minimize disturbance to sampled individuals.

Reporting for specific materials, systems and methods

We require information from authors about some types of materials, experimental systems and methods used in many studies. Here, indicate whether each material, system or method listed is relevant to your study. If you are not sure if a list item applies to your research, read the appropriate section before selecting a response.

Materials & experimental systems

n/a	Involved in the study
☒	☐ Antibodies
☒	☐ Eukaryotic cell lines
☒	☐ Palaeontology and archaeology
☐	☒ Animals and other organisms
☒	☐ Clinical data
☒	☐ Dual use research of concern
☐	☒ Plants

Methods

n/a	Involved in the study
☒	☐ ChIP-seq
☒	☐ Flow cytometry
☒	☐ MRI-based neuroimaging

Animals and other research organisms

Policy information about studies involving animals; ARRIVE guidelines recommended for reporting animal research, and Sex and Gender in Research

Laboratory animals	The study did not involve laboratory animals.
Wild animals	All study individuals were chemically immobilized for capture and collaring and subsequently released to range freely. GPS collars were removed within a year or upon low battery status.
Reporting on sex	We did not conducetsex-specific analyses because our hypotheses were at the species-scale.
Field-collected samples	The study did not involve animal samples collected from the field.
Ethics oversight	All animal handling procedures were in accordance with guidelines established by the American Society of Mammalogists. Bushbuck, nyala, and kudu handling procedures were approved by the Animal Care and Use Committees at the University of Idaho (protocol # IACUC-2019-32) and Princeton University (protocol #2075F-16). Sable handling procedures were approved by the animal ethics committee at the University of Witwatersrand (animal ethics number #2013/47/2A). Elephant handling procedures were approved by the Animal Care and Use Committee at the University of Idaho (protocol #2015-39) and by the Gorongosa Conservation Department. Lion and African wild dog handling procedures were approved by the Gorongosa Conservation Department.

Note that full information on the approval of the study protocol must also be provided in the manuscript.

Dual use research of concern

Policy information about dual use research of concern

Hazards

Could the accidental, deliberate or reckless misuse of agents or technologies generated in the work, or the application of information presented in the manuscript, pose a threat to:

No	Yes
☒	☐ Public health
☒	☐ National security
☒	☐ Crops and/or livestock
☒	☐ Ecosystems
☒	☐ Any other significant area

Experiments of concern

Does the work involve any of these experiments of concern:

No	Yes	
☒	☐	Demonstrate how to render a vaccine ineffective
☒	☐	Confer resistance to therapeutically useful antibiotics or antiviral agents
☒	☐	Enhance the virulence of a pathogen or render a nonpathogen virulent
☒	☐	Increase transmissibility of a pathogen
☒	☐	Alter the host range of a pathogen
☒	☐	Enable evasion of diagnostic/detection modalities
☒	☐	Enable the weaponization of a biological agent or toxin
☒	☐	Any other potentially harmful combination of experiments and agents